Title

Regulation of autophagy, NF-κB signaling, and cell viability by miR-124 in KRAS mutant mesenchymal-like NSCLC cells

Journal

Science Signaling, 10(496)

ISSN

1945-0877

Authors

Mehta, Anita K
Hua, Kevin
Whipple, William
et al.

Publication Date

2017-09-12

DOI

10.1126/scisignal.aam6291

Peer reviewed

HHS Public Access

Author manuscript

Sci Signal. Author manuscript; available in PMC 2017 October 26.

Published in final edited form as:

Sci Signal. ; 10(496): . doi:10.1126/scisignal.aam6291.

Regulation of autophagy, NF-κB signaling and cell viability by miR-124 in *KRAS* mutant mesenchymal-like NSCLC cells

Anita K. Mehta[1], **Kevin Hua**[1], **William Whipple**[1], **Minh-Thuy Nguyen**[1], **Ching-Ti Liu**[6], **Johannes Haybaeck**[2,3], **Joanne Weidhaas**[4], **Jeff Settleman**[5], and **Anurag Singh**[1,*]

[1]Boston University School of Medicine, Department of Pharmacology and Experimental Therapeutics, Boston, MA

[2]Medical University of Graz, Institute of Pathology, Graz, Austria

[3]Department of Pathology, University Hospital and Medical Faculty, Otto von Guericke University Magdeburg, Germany

[4]University of California at Los Angeles School of Medicine, Department of Radiation Oncology, Los Angeles, CA

[5]Calico Life Sciences, South San Francisco, CA

[6]Boston University School of Public Health, Department of Biostatistics, Boston, MA

Abstract

KRAS mutant non-small cell lung cancer (NSCLC) may be classified into epithelial or mesenchymal subtypes. Mesenchymal NSCLCs and associated “KM” cell lines are generally less responsive than their epithelial counterparts to inhibition of the RAS pathway; identifying alternative networks that promote mesenchymal NSCLC survival may lead to more effective treatments for this subtype. Non-coding microRNA (miRNA) signatures can stratify tumors into diverse molecular subtypes. By regulating numerous targets in cancer-associated signaling pathways, miRNAs can function as tumor suppressors or oncogenes. In particular, some miRNAs regulate the epithelial-mesenchymal transition (EMT). Here, we derived an EMT-related miRNA signature by profiling the abundance of miRNAs in a panel of epithelial (KE) or mesenchymal (KM) *KRAS* mutant NSCLC cell lines. This signature revealed a number of silenced or suppressed miRNAs in KM cell lines, including members of the miR-200 family, which can promote tumor suppression by inhibiting EMT. Reconstituting KM cells with one of these miRNAs, miR-124, disrupted autophagy and decreased cell survival by suppressing the abundance of p62, an adaptor for selective autophagy and regulator of the transcription factor NF-κB. Suppression of p62 by miR-124 correlated with reduced abundance of the autophagy activator Beclin 1, the ubiquitin ligase TRAF6 and the NF-κB subunit RELA/p65. Abundance of miR-124 inversely correlated with expression of *BECN1* and *TRAF6* in patient NSCLC samples. These findings identify a role for miR-124 in regulating cell survival networks in a specific subtype of

*To whom correspondence should be addressed: Anurag Singh (asingh3@bu.edu).

Author contributions: A.K.M., K.H., W.W., M.N., J.W. and A.S. conceived, designed and executed experiments followed by data analysis. Writing and review of the manuscript were performed by A.K.M., K.H., C.L., A.S., J.H., J.W., and J.S.

Competing interests: None.

KRAS mutant NSCLC cell lines, which might lead to improved subtype-selective therapeutic strategies for patients.

Introduction

Non-small cell lung cancers (NSCLCs) are aggressive and difficult to treat if diagnosed at advanced stages. A critical barrier to identifying effective therapeutics for NSCLCs, and many other related tumor types, is tumor cell plasticity that can lead to inter- and intratumoral molecular heterogeneity (1). Global gene expression profiling of NSCLCs has revealed a number of heterogeneous and contrasting molecular subtypes that associate with distinct histopathological characteristics and therapeutic vulnerabilities (2, 3). Oncogenic *KRAS* mutations are found in 20–30% of NSCLC cases, but do not stratify into a uniform molecular or histological subtype. *KRAS* mutant NSCLC cell lines display highly variable KRAS dependent transcriptional networks and cell survival pathways (4). *KRAS* mutant NSCLC cells with epithelial morphology tend to be more dependent on KRAS for survival in contrast to *KRAS* mutant mesenchymal cells, which tend to have diminished KRAS dependency. These contrasting subtypes are subsequently designated KE (epithelial) and KM (mesenchymal). The underlying molecular mechanisms that contribute to reduced KRAS dependency in the KM subtype remain unclear. It is possible that co-occurring mutations in *STK11/LKB1* and *KEAP1* along with *KRAS* may confer reduced oncogenic KRAS dependency and provoke altered sensitivity to therapeutic agents (5, 6). Indeed, many KM cell lines harbor inactivating *STK11* and/or *KEAP1* mutations. Epithelial-mesenchymal transition (EMT) is also associated with reduced sensitivity to some targeted therapeutic agents *in vitro* and drug resistance *in vivo* (1, 7).

We previously compared microarray-based gene expression data for KE and KM cell lines and derived a KE/KM gene expression signature that associates strongly with oncogenic KRAS dependency and is enriched with EMT markers such as *CDH1*/E-cadherin (4). Preliminary association studies of this signature using the Oncomine Concepts Map (8) revealed significant overlap with predicted miRNA target genes for miR-205 and miR-34. This provided rationale to determine the functional significance of altered miRNA expression patterns in the context of epithelial/mesenchymal subtypes of *KRAS* mutant NSCLC cell lines. The role of non-coding microRNAs (miRNAs) in the pathogenesis of lung cancer is highlighted by gene ablation studies of the processing enzyme *DICER1* in a genetically-engineered mouse (GEM) model of mutant *KRAS*-driven lung cancer, which causes increased aggressiveness and size of tumors (9). In some cases, the function of miRNAs can be oncogenic, as highlighted by the role of miR-21 in *KRAS*-driven lung cancer progression (10).

In human cancers, miRNAs are globally downregulated, suggesting general tumor suppressor functionality (11). A number of individual miRNAs have tumor suppressor properties, including the let-7 family, which suppress *MYC* and *KRAS* oncogene expression (12, 13). Also, the p53-regulated miR-34 family modulates some tumor suppressor functions including DNA damage response pathways (14). Lastly, the miR-200/205 family regulates epithelial-mesenchymal transition (EMT) by targeting the *ZEB1* transcriptional co-repressor

(15). Our goal was to identify miRNA gene regulatory networks that modulate epithelial differentiation and cell viability in KM subtype cells. In this study, we derived a putative KE-KM subtype miRNA signature. Subsequently, we characterized the functional role of KE-correlated miRNAs in modulating EMT, autophagy and cell death in KM subtype cells, with an overarching goal of identifying context-dependent, subtype-selective cell survival pathways that could be exploited for therapeutic benefit in the future.

Results

KE versus KM subtypes are distinguished by a miRNA expression signature

Preliminary computational analysis of a previously derived KE/KM gene expression signature (4) using the Oncomine Concepts Map showed significant overlap with predicted target genes for miR-205 (odds ratio=4.48; p=0.002) and miR-34b/c (odds ratio=3.65; p=0.002). The role of miR-205 in modulating EMT and the role of miR-34 in the p53 pathway provided rationale to investigate altered miRNA expression and function in the context of KRAS dependency and EMT subtype-associated phenotypes. To that end, we performed quantitative reverse-transcriptase PCR (qRT-PCR) Taqman low-density array (TLDA) assays to determine expression levels of 380 well-annotated mature miRNAs in a panel of 6 representative *KRAS* mutant NSCLC cell lines (Table S1) (Fig. 1). Firstly, to identify differentially expressed miRNAs in KE versus KM subtype cells, we performed student two-sided t-tests on normalized average ΔCt values (threshold cycle method) assuming unequal variances (16) for each respective miRNA in each subtype. We also calculated log2 fold differences comparing average ΔCt values for each subtype. We found that KE-correlated miRNAs were moderately higher in total number than KM-correlated miRNAs (160 versus 120 respectively) (Fig. 1A).

To select differentially expressed miRNAs, we set a slightly liberal threshold (*t*-test–derived $p < 0.1$), given the low sample size ($n = 6$) and our overarching goal of identifying miRNAs for subsequent functional studies of tumor suppressor activity. This led to the identification of 30 miRNAs that met the threshold criteria, 9 of which are correlated with KM cell lines compared to 21 KE-correlated miRNAs. To visualize co-clustered miRNA expression patterns, hierarchical clustering was performed to generate a heat map of differentially expressed miRNAs (Fig. 1B). Of note, miR-200c and miR-141, which are expressed as a tandem primary RNA transcript from a locus on chromosome 12p13.31, were co-clustered, indicating concordant expression patterns. We identified miR-205 as KE-correlated, validating the initial Oncomine analysis. We then determined whether expression of a select panel of KE-associated miRNAs was regulated by oncogenic KRAS. In H358 KE cells, siRNA-mediated depletion of KRAS reduced the abundance of specific KE-correlated miRNAs (miR-124, miR-200c, miR-141, miR-199 and miR-625) (Fig. S1A). However, in a different KE cell line (H2009) only miR-124 and miR-200c levels were reduced following KRAS depletion, whereas the others were upregulated (Fig. S1A). Therefore, one could surmise that KRAS promotes the proliferative phenotype in epithelial cells at least in part by supporting the expression of select miRNAs (such as miR-124 and miR-200c). How these miRNAs are suppressed in the KRAS-mutant mesenchymal cells, and which signaling mechanisms modulate the other EMT-associated miRNAs, remain to be determined.

Members of the miR-200 family and miR-205 regulate EMT (15), and expectedly their increased expression in KE cells and decreased expression in KM cells correlated with the abundance of epithelial and mesenchymal markers, respectively (Fig. 1C). To validate a causal role for miR-205 and miR-200c in regulating EMT in these *KRAS* mutant NSCLC lines, we performed synthetic miRNA oligonucleotide mimic transfection assays in representative KM cell lines. In H460 cells, reconstitution of miR-205 and miR-200c resulted in repression of an established target Zeb1 (Fig. 1D). Zeb1 is a C2H2-type zinc-finger protein that functions as a transcriptional repressor of the *CDH1* locus, resulting in reduced abundance of epithelial E-cadherin protein, mesenchymal differentiation and cancer stem cell-like phenotypes (17). Suppression of Zeb1 abundance by miR-200c and miR-205 was associated with increased E-cadherin protein abundance. MiR-200c reconstitution caused slightly higher E-cadherin protein induction compared to miR-205 reconstitution. Expression of the mesenchymal marker vimentin was reduced slightly upon reconstitution of high concentrations of miR-200c (Fig 1D). Compared to H460 cells, A549 cells had a greater amount of E-cadherin under control conditions, which increased moderately with miR-200c or miR-205 reconstitution and was associated with decreased abundance of Zeb1 protein (Fig. S1C). KE-correlated miRNAs did not broadly alter E-cadherin abundance in H460 KM cells; only miR-200c and miR-141 caused appreciable increases in E-cadherin protein abundance (Fig. S1D). We also observed a change in E-cadherin subcellular localization from intracellular punctate structures in control cells to more pronounced localization at cell-cell contacts in miR-200c reconstituted cells (Fig. 1E and fig. S1B). This phenotype is very similar to direct Zeb1 ablation by shRNA in KM cells (4). Finally, we validated a positive correlation (r=0.476; p=1.12e-6) between expression levels of *MIR200C* and *MIR124* primary RNA transcripts in a microarray dataset derived from primary tumors in NSCLC patients (NIH/GEO accession number GSE43458) (18). In summary, comparison of KE and KM miRNA expression profiles reveals a distinct signature, strongly associated with EMT-related molecular characteristics.

A subset of KE-correlated miRNAs causes reduced cell viability in KM cell lines

We selected a panel of 22 differentially expressed KE-correlated miRNAs based on highest fold difference from the analyses described in Fig. 1. To determine potential tumor suppressor activities of identified miRNAs, we performed comprehensive functional cell viability assays following reconstitution of KE-correlated miRNA mimics in a test set of six KM cell lines (4). We performed synthetic miRNA mimic oligonucleotide transfections and assessed cell viability effects 72 hours later (19). We noted significantly reduced cell viability following reconstitution of a number of miRNAs compared to control transfection, which varied across the cell lines tested (Fig. 2A). From this analysis, we qualitatively determined that miR-124 had generally negative effects on cell viability in all the cell lines tested. SW900 and H460 cells were generally more sensitive to the cytotoxic effects of KE-correlated miRNA reconstitutions than the other cell lines tested.

Next, we performed hierarchical clustering analysis of normalized cell viability data and generated a heat map (Fig. 2B). Cell lines could be co-clustered by similarity of responses to miRNA reconstitution, with H1792 and SK-LU-1 cells showing most concordant sensitivity patterns. H2030 and LU65 cells also showed a similar degree of concordance. We noted

some cell line specific effects, including sensitivity to miR-210 in LU65 and SW900 cells. Of note, we found that miR-205 caused minimal cell viability effects in all the cell lines tested, despite being the most significantly overexpressed miRNA in the KE subtype. In addition, miR-146b-5p and miR-125b failed to induce cell viability changes in the KM cell lines. Importantly, we identified 3 miRNAs that suppressed cell viability in all cell lines tested: miR-124, miR-518d-3p and miR-625. Of these, miR-124 had the most potent effects on reducing cell viability in all KM cell lines.

MiR-124 reconstitution induces apoptosis and suppresses clonogenic growth of KM cell lines

To further elucidate cytotoxic mechanisms caused by reconstitution of KE-correlated miRNAs in KM cell lines, we used a luminescent caspase-3-Glo™ reporter assay to measure effects on apoptosis. Increased luminescence in this assay is proportional to increased effector caspase-3 activation. We tested 3 miRNAs (miR-124, miR-199a, and miR-625), which all caused increased caspase-3 activation in H460 KM cells (Fig. 3A). Of these, miR-124 caused the strongest caspase-3 activation compared to miR-199a and miR-625. In contrast, caspase-3 activity was weakly induced or absent in *KRAS* wild-type H322 NSCLC cells and MCF7 breast cancer cells (Fig. 3A).

Given that, among the KE signature miRNAs tested, miR-124 had the greatest cytotoxic effects in KM cells, we focused our subsequent efforts on investigating miR-124. To determine whether the cytotoxic effects of miR-124 conferred reduced clonogenic growth, we transduced A549 KM cells with a lentiviral vector encoding the primary form of miR-124 (pri-MIR124). The MCF7 breast cancer cell line, which again have wild-type KRAS, were transduced alongside as a control. We then performed 3D culture assays of stable cell lines in Matrigel™. A549 cells expressing miR-124, when grown in Matrigel™, displayed signs of cytotoxicity manifesting as reduced size and number of colonies (Fig. 3, B and C). Furthermore, nuclear DNA fragmentation indicative of cell death could be observed in many of the miR-124 expressing cells (Fig. 3B). In contrast to A549 cells, there were no changes in colony size and numbers in MCF7 cells expressing miR-124 (Fig. S2, A and B). Reconstitution of miR-124 in H460 cells caused increased caspase-3 cleavage in 3D cultures, as determined by immunofluorescence microscopy (Fig. S2C), and reduced clonogenic growth in monolayer cultures (Fig. S2D). Finally, miR-124 mediated cytotoxicity was associated with distinct morphological features, including the appearance of dense intracellular vacuolar structures (Fig. 3D). This indicated a possible perturbation of lysosomal function, perhaps as a consequence of altered regulation of macroautophagy, referred to hereafter as autophagy. Constitutive activation of the cytoprotective autophagy pathway drives survival in subsets of *KRAS* mutant mesenchymal-like cancer cell lines (20). This prompted our interest in investigating a context-dependent role for miR-124 in perturbation of autophagy pathway activation in KM cells.

MiR-124 reconstitution causes autolysosomal maturation defects in KM cells

A number of assays and guidelines have been developed and established to study activation of autophagy and so-called “flux” through the pathway (21). To monitor autophagy flux in cells reconstituted with miR-124, we used a common dual fluorescent LC3 reporter, which

is expressed as an amino-terminal fusion of mCherry and GFP to human LC3B (Fig. 4A) (22). Activation or inhibition of the autophagy pathway is determined by quantitating LC3 aggregates by live-cell fluorescence microscopy. Overlap of red and green signals from mCherry and GFP, respectively, will appear as yellow aggregates upon induction of phagophore formation and autophagosome accumulation. If the autophagy pathway is in flux, these yellow aggregates will be transient as autophagosomes (AP) fuse with acidic lysosomes to form autolysosomes (AL) in which the low pH quenches GFP fluorescence resulting in rapid accumulation of dense red aggregates (Fig. 4A).

We introduced mCherry-GFP-LC3 (mCG-LC3) into H460 cells by stable retroviral transduction to monitor LC3 dynamics in live cells in real time. These cells were transfected with miR-124 mimics either alone or in combination with the lysosomotropic agent hydroxychloroquine (chloroquine), which causes rapid deacidification of lysosomes and a subsequent block in autophagosome/lysosome fusion. Live-cell imaging of mCG-LC3 aggregates over 72h following addition of agents to H460 cells revealed dynamic alterations in autophagy flux induced by miR-124 and/or chloroquine compared to control cells (Fig. 4B, and fig. S3A). In control cells, some green/yellow AP puncta were seen transiently. These AP puncta dissipated over several hours and, as cell density increased over 48–50 hours, red AL aggregates began to form and accumulate (Fig. 4B first row, fig. S3A and Movie S1). In miR-124 reconstituted cells, overall GFP fluorescence was weak, but yellow AP aggregates began to form around 22 hours after transfection (Fig. 4B, second row and Movie S2). Of note, the AP aggregates appeared as single large aggregates per cell. These aggregates persisted for an additional 8h to 20h and eventually dissipated. Cells with accumulated AP aggregates underwent cell death at 48h to 50h post-transfection. Chloroquine treatment caused formation and accumulation of dense AP aggregates, as expected based on previous reports (Fig. 4B, third row and Movie S3) (23). Chloroquine-induced AP aggregates persisted for 50 hours, with some undergoing mild AL maturation. The AP aggregates in chloroquine-treated cells were more numerous and smaller per cell, in contrast to miR-124 reconstituted cells. Chloroquine treatment alone had mild cytotoxic effects in H460 cells. When combined with miR-124 reconstitution, chloroquine promoted synergistic cell death (Fig. 4B and Movie S4).

We performed software based image cytometry and set thresholds to identify and count LC3 aggregates based on size and fluorescence intensity. AP and AL puncta were identified by setting appropriate empirically-derived thresholds for mCherry and GFP fluorescence (fig. S3B). To increase the accuracy of puncta identification and quantification, “gating” was performed to isolate high green and high red fluorescent AP puncta in contrast to low green and high red fluorescent AL puncta. In control cells, AP counts remained at a steady-state low level (Fig. 4C). MiR-124 reconstitution caused a mild increase in AP counts, whereas chloroquine treatment caused a significant steady time-dependent increase in AP accumulation, as expected, since chloroquine blocks AP to AL maturation. Chloroquine treated cells showed accumulation of multiple APs per cell. In contrast, in miR-124 reconstituted cells, chloroquine induced AP accumulation was severely blunted approximately 10h post-transfection. Control cells showed robust AL accumulation over time, consistent with constitutive basal activation of autophagic flux in these cells. Reconstitution of miR-124 caused a noticeable effect on blocking AL accumulation (Fig.

4D). This latter effect on blocking AL formation by miR-124 was comparable to the effects of chloroquine. This effect of miR-124 on blocking AL accumulation was additive when combined with chloroquine (Fig. 4D). Calculation of AL:AP ratios further demonstrated relatively high AL accumulation in control cells, which was severely impaired in chloroquine treated cells and moderately impaired in miR-124 transfected cells (Figure 4E). In summary, miR-124 causes defects in AP maturation and AL accumulation in H460 KM cells. Mir-124 combined with chloroquine causes enhanced blockade of AP and AL accumulation, which is accompanied by additive cytotoxic effects.

MiR-124 suppresses p62 and beclin-1 abundance selectively in KM cells

To determine mechanisms underlying miR-124 mediated regulation of the autophagy pathway, we analyzed the abundance of key autophagy pathway protein components after miR-124 reconstitution, including *SQSTM1*/p62 and LC3-I/II, which are well-established markers of pathway activation (24). Firstly, we validated that reconstitution of miR-124 induced apoptosis in all KM cell lines tested, as assessed by increased levels of cleaved PARP. Expression of beclin 1, which initiates phagophore formation and promotes autolysosome maturation (25, 26), was suppressed in all four KM cell lines by miR-124 (Fig. 5A). We used the TargetScan web portal to identify a high probability predicted target site for miR-124 in the 3′UTR of *beclin1/BECN1* mRNA (table S2). We confirmed that miR-124 directly targets the 3′UTR of *BECN1* using an engineered luciferase reporter construct whose luminescence was reduced 40% by miR-124 reconstitution compared to control transfected cells, whereas miR-200c reconstitution failed to cause significant effects on reporter activity (fig. S4A). Furthermore, exogenous expression of beclin-1 in A549 cells caused a mild 10 percent rescue of miR-124 dependent cell proliferation defects (fig. S4B). Beclin 1 expression also partially rescued effects on PARP cleavage and LC3-II accumulation following miR-124 reconstitution (fig. S4, C and D). Finally, *BECN1* and *MIR124* expression were inversely correlated in primary NSCLC tumor samples from patients (fig. S4E, r=−0.44; p=4.35e-5).

Next, we found that miR-124 induced altered expression of ATG16L1, with increased abundance of the shorter α protein variant, which has previously been associated with impaired AP maturation (Fig. 5A) (27). In addition, miR-124 caused robust suppression of the selective autophagy adaptor protein p62. These effects of miR-124 were associated with increased expression of LC3-II, indicating a block in AL function, since LC3-II degradation and turnover are mediated by AL activity. Furthermore, immunofluorescence microscopy of p62 expression showed that miR-124 caused significant reduction in the number and size of p62 aggregates in H460 cells (fig. S5, A and B). TargetScan analysis of the *SQSTM1* 3′ UTR also showed a predicted miR-124 target seed sequence (table S2). The effects of miR-124 on the autophagy pathway correlated with reduced abundance of phosphorylated S6 at $Ser^{235/236}$, indicating perturbation of mTOR/S6K or ERK/RSK kinase activity (fig. S5C). Reduced *SQSTM1* mRNA abundance upon miR-124 reconstitution was validated by qPCR (fig. S5D). Reduced p62 abundance is usually associated with increased rather than decreased autophagic flux. We suggest that miR-124 blocks autophagosome formation and maturation via suppression of beclin 1, concomitant with suppression of p62 abundance.

To provide further supportive evidence for a role of miR-124 in blocking autolysosome formation and function, we analyzed expression levels of another selective autophagy adaptor protein, NBR1, which is involved in selective autophagic degradation of some ubiquitinated cargo proteins (28). Reconstitution of miR-124 caused increased NBR1 protein abundance in a panel of KM cell lines. This was associated with increased LC3-II levels, indicative of reduced AL function, consistent with the aforementioned data showing that miR-124 causes a block in AL accumulation (Fig. 4D). Subsequently, we investigated the effects of combining chloroquine with miR-124 reconstitution on NBR1 protein levels in H460 cells (Fig. 5B). Chloroquine treatment caused increased p62 protein levels, consistent with a block in AL function. This effect was abrogated by combined reconstitution of miR-124 with chloroquine treatment. Under the same conditions, NBR1 abundance was additively increased. Surprisingly, we found that chloroquine treatment alone did not promote an increase in the amount of NBR1. The reasons for this are unclear, given that p62 protein abundance was markedly greater in chloroquine-treated cells. Nonetheless, the findings indicate that miR-124 inhibits selective autophagy by blocking autolysosome formation and function.

Given the sensitivity of mesenchymal cell lines to miR-124 reconstitution, we investigated a causal role for EMT in modulating this sensitivity. Whereas miR-124 induces apoptosis in H460 KM cells, as assessed by increased abundance of cleaved PARP, there was no such apoptotic response in the KE H358 cell line (Fig. 5C). Interestingly, miR-124 caused suppression of vimentin abundance in both H460 and H358 cells. Based on TargetScan analysis, the *VIM* mRNA (encoding vimentin) harbors a predicted miR-124 target site in the 3′UTR (table S2). Of note, p62 abundance was decreased only in H460 KM cells but not in H358 KE cells (Fig. 5C). This could be due to additional p62 regulatory mechanisms that are active in KM cells.

To establish a causal role for EMT in mediating sensitivity to miR-124 reconstitution, we used a stable mesenchymal variant of the H358 cell line, designated H358M (4). In contrast to H358 cells, H358M cells were more sensitive to miR-124 reconstitution as assessed by more prominent PARP cleavage indicative of apoptosis. Gross morphological cytotoxicity could also be observed in miR-124 reconstituted H358M cells, which was not apparent with the parental H358 cells (fig. S5E). As with H460 KM cells, miR-124 suppressed vimentin and p62 levels in H358M cells (Fig. 5D). The sensitivity of H358M cells to miR-124 was associated with decreased levels of mature miR-124 RNA levels in H358M compared to parental H358 cells (Fig. 5E). Finally, to determine if miR-124 had cross-tissue effects on p62, we investigated effects in *KRAS* mutant mesenchymal pancreatic ductal adenocarcinoma (PDAC) cell lines, KP1N and KP4 (fig. S5F). As with NSCLC KM cells, miR-200c caused increased E-cadherin expression in PDAC KM cells. Mir-124 reconstitution caused p62 suppression in PDAC cell lines, similar to effects in NSCLC cell lines.

In addition to p62, we identified other putative miR-124 target genes, including beclin 1 (see fig. S4) and vimentin, lending uncertainty to which target genes mediate the phenotypic effects of miR-124 in KM cells (table S2). Therefore, we determined if miR-124 directly suppresses SQSTM1/p62 expression by binding the 3′ UTR of p62 mRNA and whether this

suppression was responsible for the cytotoxic effects observed in KM cell lines. Firstly, we noted that H460 cells were sensitive to siRNA mediated depletion of p62 as assessed by PARP cleavage-associated cell death, which was not evident in the H358 KE cell line (fig. S5G). This indicates that p62 drives anti-apoptotic signaling in H460, and possibly other KM cell lines. Secondly, we performed a luciferase based assay with a lentiviral reporter vector containing the entire 3′ UTR of human *SQSTM1* mRNA downstream of LUC/ luciferase gene driven by an EF1α promoter (Fig. 5F). To functionally validate the predicted seed sequences for miR-124 in the *SQSTM1*-3′ UTR, we tested the effects of miR-124 on reporter activity of either wild-type or mutated miR-124 target site seed sequences (Fig. 5F). Introduction of miR-124 resulted in a 50% reduction in the reporter gene activity of the *SQSTM1* 3′ UTR containing wild-type miR-124 targeting sequences (Fig. 5F). In contrast, two different mutated *SQSTM1-3′ UTR* sequences did not respond significantly to miR-124 mediated luciferase suppression. Lastly, we performed rescue experiments using exogenous expression of GFP-tagged p62, that lacks the endogenous *SQSTM1* 3′UTR sequence (fig. S5H). Exogenous expression of GFP-p62, which is resistant to suppression by miR-124, rescued the cell viability defects caused by miR-124 reconstitution in SW900 and A549 KM cell lines (Fig. 5G). In summary, we conclude that cytotoxic effects of miR-124 are selective for KM subtype cells via coordinated effects on the autophagy pathway and apoptosis induction, with p62 as a central hub in the miR-124 regulatory network.

NF-κB signaling and cytokine expression are regulated by miR-124

In addition to a role in autophagy, p62 is critical for activation of the nuclear factor–κB (NF-κB) transcriptional complex and downstream effects on inflammatory cytokine signaling (29). We found that expression of the p65 subunit (*NFKB1/RELA*) of NF-κB was suppressed following miR-124 reconstitution. This was accompanied by reduced abundance of the E3 ubiquitin ligase TRAF6, which mediates IκB kinase (IKK) and subsequent NF-κB activation (Fig. 6A) (30). The TargetScan portal returns TRAF6 and p65/*RELA* as predicted miR-124 target genes (Table S2). Furthermore, *TRAF6* and *MIR124* mRNA abundance were inversely correlated in primary NSCLC samples (Fig. S6A, r=−0.62; p=8.45e-10). We verified that miR-124 caused reduced NF-κB signaling by using a κB binding element-firefly luciferase construct. In A549 and SW900 KM cells, we observed two to three-fold decreases in NF-κB transcriptional activity following miR-124 reconstitution (Fig. 6B).

Given the role of NF-κB in regulating inflammatory cytokine signaling, we hypothesized that cytokine expression levels might be altered in miR-124 reconstituted KM cells. Indeed, conditioned media from miR-124 reconstituted KM cells contained altered levels of key cytokines compared to NC control transfected cells (Fig. 6C). Quantitation of cytokine levels revealed proinflammatory cytokines such as TNFα and IL-1α were increased upon miR-124 reconstitution in KM cells. Other induced factors included TGFβ, IL-12, RANTES, IL-11, IFNγ and IL-6 (Fig. 6C). Conversely, GMCSF, IL-4, IL-10 and soluble TNF decoy receptor (sTNFRI/II) were decreased upon miR-124 reconstitution. We verified that alterations in cytokine expression upon miR-124 reconstitution occurred due to changes in mRNA levels of key cytokines as assessed by qRT-PCR in the miR-124 reconstituted KM cells. We noted strong mRNA induction of *IL1B*, *IL11* and *TNF*, but surprisingly saw reduced *IL6* expression (fig. S6B). In summary, miR-124 reconstitution promotes

suppression of TRAF6-NF-κB signaling and associated perturbations in pro- and anti-inflammatory cytokine expression levels.

Discussion

In this study, a KE/KM subtype miRNA signature was derived by differential miRNA expression profiling. The signature reveals EMT regulatory miRNAs such as miR-205 and miR-200c, as well as a number of cytotoxic miRNAs such as miR-124, which are expressed at significantly lower levels in KM cell lines compared to KE cell lines. Importantly, we demonstrate miR-124 negatively regulates cell viability in several KM cell lines upon functional reconstitution. Induction of cell death upon miR-124 reconstitution is associated with the formation of dense vacuolar structures suggesting perturbations in lysosomal turnover and possible defects in autophagy. Autophagy is constitutively activated in subsets of *KRAS* mutant cancers and cell lines in large part via transcriptional mechanisms (31). This is associated with maintenance of cell viability, suggesting a possible therapeutic vulnerability in *KRAS* mutant cancers (32). Our findings indicate that *KRAS* mutant cells with mesenchymal differentiation exhibit constitutive flux through the autophagy pathway and are particularly sensitive to perturbation of this flux, for example via reconstitution of miR-124.

Selective autophagy is promoted by beclin 1 and specific cargo are targeted for degradation by the adapter protein sequestosome1/p62 (33, 34). We conclude that suppression of beclin 1 and p62 by miR-124 is associated with defective AL maturation and accumulation. The defect in AL formation caused by miR-124 is supported by three independent experimental observations. Firstly, miR-124 reconstitution prevents AL accumulation as demonstrated by live cell imaging of the fluorescent mCherry-GFP-LC3 reporter. Secondly, LC3-II protein levels accumulate upon miR-124 reconstitution indicating a defect in AL function, which normally promotes LC3 degradation and turnover. Lastly, levels of another selective autophagy adaptor NBR1 accumulate following miR-124 reconstitution. NBR1 is critical for turnover of a number of ubiquitinated target proteins via autolysosomal degradation (28).

Concomitant with perturbation of AL accumulation, suppression of p62 leads to cell death in KM cell lines. This observation is concordant with previous studies that demonstrate a role for p62 in mutant *RAS*-driven tumor maintenance (35). The mechanisms by which p62 promotes the survival of KM cell lines is complex and may involve coordinated control of selective autophagy and activation of the NF-κB pathway. P62 binds to cargo targeted for degradation via the selective autophagy pathway, which include ubiquitinated proteins and damaged organelles (24, 34, 36). We also implicate beclin 1 as a key miR-124 target. We hypothesize that miR-124 dependent suppression of beclin 1 causes defects in formation of mature ALs, which partially contributes to cytotoxic effects. Our findings support the notion that autophagy activation in *KRAS* mutant cancer cells plays a pro-tumorigenic role. These findings contrast with studies indicating tumor suppressor roles for the autophagy pathway, as demonstrated by a tumor predisposition phenotype in mice with *Becn1* heterozygous loss (37). Context and molecular subtype dependence of oncogenic versus tumor suppressor roles for the autophagy pathway is a contentious issue and will need to be reconciled for the design and clinical use of autophagy inhibitors.

Our findings on the role of miR-124 in autophagy regulation are reinforced by previous studies demonstrating significant enrichment for miR-124 predicted target sites in a number of autophagy-lysosomal pathway genes (38). In addition to targeting of p62, and beclin 1, we found that miR-124 targets vimentin expression, which is an established mesenchymal cell marker protein. Studies show that vimentin can regulate autophagy by tethering an inhibitory AKT-phosphorylated beclin 1 in complex with 14-3-3 protein (39). Thus, miR-124 inhibits multiple steps in the autophagy pathway. Of all the putative miR-124 targets, our results strongly implicate *SQSTM1*/p62 as the most critical gene for maintenance of KM cell survival, as demonstrated by rescue experiments.

Reduced p62 levels are commonly associated with increased autophagy flux, which promotes p62 autolysosomal degradation (33). We found that miR-124 dependent suppression of p62 is associated with increased NBR1 and LC3-II levels and a decrease in AL accumulation, indicative of a block in autophagy. How can these findings be reconciled? We hypothesize that miR-124 disrupts the formation and enclosure of autophagosomes, as occurs following beclin 1 or Vps34/Class III PI3K gene ablation (40). When miR-124 is expressed, p62 levels are decreased perhaps via destabilization of *SQSTM1*/p62 mRNA. Beclin 1 also regulates AL maturation via sequestration of the negative autophagy regulator Rubicon (26). Therefore, miR-124 dependent suppression of beclin 1 could cause AL maturation defects leading to increased LC3-II and NBR1 levels. The miR-124 dependent block in autophagy is seen selectively in KM cell lines, since miR-124 introduction into KRAS WT cells and H358 KE cells fails to induce increased LC3-II levels. The mechanistic basis for selective p62 suppression and dependency in KM subtype cells remains unclear and will be interesting to explore in future studies.

The effects of miR-124 mediated suppression of p62 on cell viability are likely to involve disruption of multiple pathways, including negative regulation of autophagic flux. A recent study indicates loss of cell viability in A549 and H460 KM cell lines can be induced by combined disruption of autophagy and the oxidative pentose phosphate pathway. This latter pathway could be subject to perturbation by miR-124 as a mechanism underlying cell death induction (41). Furthermore, loss of p62 function has been linked to metabolic disruption in some contexts (42). Therefore, metabolic reprogramming could be a mechanism to explain the cytotoxic effects of miR-124 reconstitution in KM cells, which will be an interesting avenue to explore in future studies.

In addition to functioning as a selective autophagy adaptor, p62 regulates inflammatory signaling via IκB kinase (IKK) dependent activation of the NF-κB pathway (35). We show that miR-124 reconstitution promotes *NFKB1*/p65 suppression, leading to reduced NF-κB transcriptional activity and altered expression of key cytokines. This is consistent with a previous study identifying miR-124 as the top negative regulator of NF-κB in a miRNA mimic functional screen (43). Whether this is a direct suppression of the p65 3′ UTR by miR-124 remains unclear. Mechanistic association between activation of autophagy and inflammatory responses have been documented. For example, pathogenic antigen phagocytosis in macrophages is associated with increased LC3 aggregation on APs, which is critical for innate immune responses (23). Furthermore, germline *ATG16L1* mutations are causally associated with increased intestinal inflammation seen in Crohn's disease (44). We

found that miR-124 reconstitution induces differential expression of the ATG16L1α isoform, which could feed into regulation of inflammatory signaling.

Interestingly, *KRAS/TP53* co-occurring mutations, reflective of the KE subtype, correlate with increased proinflammatory signaling whereas *KRAS/STK11* or *KRAS/KEAP1* mutations associate with increased anti-inflammatory signaling, for example via constitutive activation of the Nrf2 anti-oxidant pathway (5). Thus, activation of anti-inflammatory signaling is generally observed in a subset of KM cells that harbor *STK11* and *KEAP1* mutations such as A549 and H460 cells. Taken together, our studies have defined a NSCLC subtype specific regulatory mechanism that controls the coordinated function of the autophagy and NF-κB signaling pathways, with p62 as a central and critical hub in the network (Figure 7). From a therapeutic perspective, miRNA reconstitution is currently being tested in pre-clinical and early phase clinical trial settings (45). Thus, reconstitution of miR-124 and other KE-correlated miRNAs may prove beneficial for a subtype of NSCLC that has molecular characteristics of KM cell lines.

Materials and Methods

Quantitative profiling of miRNA expression in cell lines

Cells were grown to confluency in 60mm dishes, trypsinized and pelleted. Total RNA was extracted from cells using the Qiagen miRNeasy kit. MiRNA expression was quantitated by quantitative reverse-transcriptase PCR (qPCR) using Taqman Low-Density Arrays (TLDA) as described previously (46). Raw TLDA data is shown in Table S1 and is publically available via the NIH Gene Expression Omnibus online portal (accession # GSE102298). Expression data were processed in MS Excel to generate a volcano plot and to identify differentially expressed miRNAs in KE versus KM cells. Data were further processed in “R” equipped with the “pheatmap” package to perform hierarchical clustering and to generate a heat map of differentially expressed miRNAs.

Quantitative PCR assays for miRNA and mRNA abundance

Abundance of mature miRNAs in cell lines was measured using the miScript qRT-PCR system (Qiagen Inc.). Briefly, cells were lysed in Qiazol reagent following transfection with siKRAS (48h post-transfection) or under control conditions. Total RNA was extracted using the miRNeasy kit. Total RNA (2μg) was reverse transcribed using the miScript HiFlex buffer, to generate cDNA for small non-coding RNA as well as mRNA. PCR assays were performed on 1:50 diluted cDNA using sequence specific primers and the Quantitect SYBR Green PCR mix. PCR products were detected using an Applied Biosystems Step One Plus instrument. Threshold cycle (Ct), ∂Ct and ∂∂Ct were generated with the Step One Plus software. Data were normalized to abundance of endogenous *SNORD6* RNA for miRNA quantitation, or to *GAPDH* abundance for mRNA quantitation.

Cell lines, miRNA mimics and siRNA transfections

Human cancer cell lines (H460, A549, SKLU1, H2030, SW900, H1792, LU65, SW1573, H2009, H322, H358, H358M, H441, MCF7) were grown in RPMI supplemented with 5% FBS (heat-inactivated at 50°C), 1mM Sodium Pyruvate and penicillin/streptomycin as

described previously (4, 47). For initial small scale screening, miRNA mimic and NC control dsRNA oligonucleotides were purchased from Dharmacon Inc. in 96-well arrayed format. Cells were transfected with RNAiMax reagent (Invitrogen) at 10nM. For subsequent follow-up studies, NC and miRNA mimics were purchased from Qiagen and transfected at 10 or 50nM for signaling pathway analyses by Western blotting. SiRNA (dsRNA) oligonucleotides against *SQSTM1* and *KRAS* were obtained from IDT and used at 10nM final concentration in media.

Cloning of the pri-MIR124 lentiviral vector

Genomic DNA from 293T cells was used as template to PCR amplify the human primary MIR124-2 gene sequence (chr 8p12.3) using flanking forward/attB1 and reverse/attB2 Gateway cloning adapter primers (Table S3). A 2-step Gateway PCR protocol was employed to clone the MIR124-2 605 nt sequence into pDONR-223 and then into a Gateway compatible pWPI lentiviral vector backbone (gift from Didier Trono, Addgene plasmid #12254) using BP and LR clonases, respectively. Cloned sequences were verified by automated DNA sequencing. All viral vectors were packaged and generated in 293T cells using previously described methods (4, 48).

UTR reporter plasmid cloning and luciferase assay

A 1.2 kB DNA fragment corresponding to the 3′ UTR of *SQSTM1*, with putative miR-124 binding sites, was PCR amplified from human 293T cell genomic DNA by PCR using forward and reverse Gateway adapter primers (Table S1). Mutant 3′ UTR sequences lacking the critical base-pair complementarity within the 8-mer miR-124 seed sequence was generated by site-directed mutagenesis using the QuikChange kit (Agilent Inc., La Jolla, USA). *SQSTM1 3′* UTR DNA fragments were cloned into a modified pWPI lentiviral vector containing an upstream firefly luciferase gene driven by an EF-1α promoter. All clones were sequence verified by DNA sequencing. For luciferase assays, cells were transduced with WT or mutant pWPI-*SQSTM1* 3′UTR lentiviral vectors. A similar approach was employed for cloning of the *BECN1* 3′UTR. LUC-3′UTR transduced cells were plated in 96 well plates at 5×10^3 cells/well. After 12 hours, these cells were transfected with miR-124 mimics or non-target controls (NC) at 50nmol/μL with Lipofectamine RNAiMAX (Invitrogen) according to manufacturer recommendations. Two days post-transfection, cells were treated with 100μg/ml D-luciferin and incubated at 37°C for 5 minutes and “glow-based” luminescence was measured with Fluostar Optima plate reader (BMG Labtech) with a 5 s integration time. Relative luciferase activity was normalized to the vector control (pWPI-luciferase vector) and NC miRNA mimic control.

Cell viability and apoptosis assays

Cells were plated in 96 well plates at 5×10^3 cells/well. Cells were transfected with miRNA mimics or NC control 18–24 h post-plating. Cell viability assays were performed by adding Alamar Blue (Resazurin) reagent at 6.5μg/ml and incubated for 30 minutes at 37°C. Converted Resafurin fluorescence was measured at $\lambda_{Ex}/\lambda_{Em}$ 590nm using a Fluostar Optima plate reader. Cell viability was normalized to control transfected cells. For caspase 3 activity based apoptosis assays, cells were plated in white 96 well plates and transfected with miRNA mimics as described above. Caspase 3 activity was measured using the

luminescence-based Caspase-Glo 3/7 assay (Promega Inc.) 48 hours after transfection, by directly adding 25μL of the caspase assay mix to cells. Luminescence was measured using a Fluostar Optima plate reader, with a 10 sec. integration time. For p62 and beclin 1 rescue experiments cells were transduced with GFP-p62 (pMXs-puro GFP-p62 was a gift from Noboru Mizushima - Addgene plasmid # 38277) or pLEX-BECN1. Stable polyclonal cell populations were selected in puromycin (1μg/ml) for 1 week. Stably-transduced cells were plated in 96 well plates and transfected with miR-124 or NC at 50nM. After 72 h, cell viability was assessed using the Alamar Blue assay as described above.

Clonogenic and Matrigel assays

For clonogenic assays, 5×10^3 cells were plated in 6-wells plates and transduced with control or miR-124 lentiviral vectors. Transduced cells were plated at 500 cells per 60mm dish. Clones were grown for 2 weeks, fixed in EM grade 4% formaldehyde and stained with Giemsa dye according to manufacturer guidelines. For 3D clonogenic growth assays in Matrigel, control or miR-124 transduced cells were plated in 8-well chamber slides (NUNC Inc.) using a bottom layer “on-top” method as described previously (49). Colonies were allowed to form for two weeks with media change every alternate day. Colonies were imaged by bright field microscopy and CellProfiler software (50) was used to determine colony counts and size. Colonies were fixed in EM grade 4% formaldehyde and stained with DAPI and phalloidin. For cleaved caspase detection, colonies were permeabilized with 0.1% Triton X-100 and incubated with cleaved caspase-3 primary antibody (Cell Signaling Inc.) overnight. Anti-rabbit secondary antibody conjugated to Alexa-594 was used for immunofluorescence detection. Images were acquired with a Cytation 3 imaging system (BioTek Inc.) equipped with 10X objective lens. Raw tif files were processed in Adobe Photoshop to adjust color balance and levels.

Immunofluorescence Microscopy

Cells were fixed in 4% EM grade formaldehyde and permeabilized with 0.1% Triton X-100. Cells were stained with primary antibodies against vimentin, E-cadherin, p62 overnight at 4°C followed by fluorescent-labeled Alexa488 or Alexa594 conjugated goat anti-mouse/ anti-rabbit secondary antibodies (Molecular Probes). Spheroids in Matrigel were fixed as described previously (49) and stained with Alexa594 conjugated phalloidin to stain actin filaments (Thermo Fisher Scientific), DAPI or Hoechst 33256 dyes were used to stain nuclear DNA. Leica SP5 Laser Confocal Microscope equipped with a 63X Oil objective (Fig. 3B and S2A) was used for image acquisition. Micrographs shown in Fig. 1E and fig. S1B were captured on an Olympus IX81 Spinning Disk Deconvolution Microscope equipped with a 40X Plan-Apo Oil objective lens. Digital images were processed with Slidebook. Images were compiled and further processed with NIH Image J, Adobe Illustrator and Photoshop CS6.

Western Blotting and Antibodies

Protein lysates were prepared with 1X Laemlli Buffer followed by 15s pulse sonication. Lysates were normalized for total protein content using BCA assay reagent (Pierce-Thermo). Proteins were separated by SDS-PAGE followed by transfer to PVDF membranes. Enhanced chemiluminescence (ECL) with West-Pico or West-Dura reagents (Pierce-Thermo). Syngene

G-Box XT4 system and GeneSys software was used for ECL imaging. The following antibodies were used for Western blotting: Cleaved-PARP (Cell signaling, 1:1000), Zeb1 (Santa Cruz, 1:1000), E-cadherin (BD Biosciences, 1:1000), vimentin, phospho-S6, t-S6, Beclin 1, Atg16L1, p62/Sqstm1, LC3-I/II, p65/NFkB1, NBR1 (Cell Signaling, 1:1000) and GAPDH (Santa Cruz, 1:5000). All antibodies were diluted in 2% BSA/TBS-T solution.

Autophagy live cell imaging

Cells stably expressing dual reporter pBabe-puro mCherry-EGFP-LC3B (22) were plated at 5×10^3 density in 12 well plate format in phenol red free RPMI-1640/5% FBS. 24 hours post seeding cells were transfected with miR-124 or NC oligos. 6 hours post transfection these cells were treated with 50 μM chloroquine. Live cells maintained at 37°C and 5% CO^2 were imaged in a Cytation 3 imaging system (BioTek Inc.) equipped with 10X objective lens for 72 hours. Nine fields per well were selected and images were taken at an interval of every 20 minutes using laser autofocusing. GFP or mCherry fluorescence were imaged using LED filter cubes with $\lambda_{Ex}/\lambda_{Em}$ 469/525nm and 586/647nm respectively. Gen5 imaging software was used to identify and quantitate green and red LC3 puncta by setting empirically derived thresholds. Fluorescence intensity cutoffs were established to specifically count green/red puncta (autophagosomes/APs) or red puncta alone (autolysosomes/ALs).

miRNA isolation and measurement

Total RNA from cells was isolated using the miRNeasy mini kit (Qiagen) according to manufacturer guidelines. 1μg total RNA was transcribed to cDNA by using miScript II reverse transcription kit (Qiagen). Diluted cDNA (50X) was used in miScript primer assays (Qiagen). Relative expression levels of mature miRNA were analyzed by real time quantitative PCR (qPCR) in a StepOne Plus system (Applied Biosystems Inc.). U6 snRNA was used as endogenous small RNA control for miRNA normalization and relative expression levels of miRNAs were calculated using the $2^{-\Delta\Delta ct}$ method after normalization (16).

Cytokine expression array analyses

$1{\times}10^6$ cells were plated in RPMI/0.5% FBS in 150 mm dishes. After 24 h, cells were transfected with 50nM control or miR-124 mimic. 48 h post-transfection, conditioned media was collected and concentrated 20-fold with 3kDa Centrifugal Filter Units (Millipore). Concentrated media was applied to human inflammation antibody array C3 (Ray Biotech Inc.) to detect cytokines according to manufacturer guidelines. Antibody binding was visualized and quantitated by ECL with the Syngene G-Box XT4 system/GeneSys software. Data analysis was performed using NIH Image J and a dot blot analyzer plug-in. Dot intensity data were normalized and processed in Microsoft Excel.

Statistical analyses

Statistical and computational analyses were performed using “R” or Graph Pad Prism. Analyses were verified and validated by Dr. Ching-Ti Liu (Department of Biostatistics, Boston University School of Public Health). For parametric tests on normally distributed data, we performed student two-sided t-tests assuming unequal variances. Colony size data

in Fig. 3C were compared using the non-parametric Mann-Whitney test. Where indicated, ** denotes $p < 0.01$ and *** denotes $p < 0.001$. For correlation analyses of gene expression microarray data derived from primary tumors in NSCLC patients (NIH/GEO accession number GSE43458), RMA normalized data were generated in R and individual gene level data for *MIR124, MIR200C* (primary transcripts), *BECN1* and *TRAF6* were extracted. Pearson correlation coefficients and associated p values for pairwise gene expression comparisons were calculated in R using cor.test. Scatter plots were generated with the ggplot package in R.

Supplementary Material

Refer to Web version on PubMed Central for supplementary material.

Acknowledgments

We thank our colleagues, Dr. Neil Ganem, Dr. Hui Feng and Dr. Rachel Flynn and their research teams for discussions and advice on the project. We thank Dr. Rushika Perera (UCSF School of Medicine) for critical evaluation of the manuscript.

Funding: This work was supported by NIH/NCI R00 CA149169, American Lung Association Lung Cancer Discovery Award and an American Cancer Society IRG Pilot Award to A.S. as well as NIH T32 GM008541 to K.H. A.M. and A.S. are partially supported by the Shamim and Ashraf Dahod Breast Cancer Center at BUSM.

References and Notes

1. Sequist LV, Waltman BA, Dias-Santagata D, Digumarthy S, Turke AB, Fidias P, Bergethon K, Shaw AT, Gettinger S, Cosper AK, Akhavanfard S, Heist RS, Temel J, Christensen JG, Wain JC, Lynch TJ, Vernovsky K, Mark EJ, Lanuti M, Iafrate AJ, Mino-Kenudson M, Engelman JA. Genotypic and histological evolution of lung cancers acquiring resistance to EGFR inhibitors. Sci Transl Med. 2011; 3:75ra26.
2. Bild AH, Yao G, Chang JT, Wang Q, Potti A, Chasse D, Joshi MB, Harpole D, Lancaster JM, Berchuck A, Olson JA Jr, Marks JR, Dressman HK, West M, Nevins JR. Oncogenic pathway signatures in human cancers as a guide to targeted therapies. Nature. 2006; 439:353–357. [PubMed: 16273092]
3. Hayes DN, Monti S, Parmigiani G, Gilks CB, Naoki K, Bhattacharjee A, Socinski MA, Perou C, Meyerson M. Gene expression profiling reveals reproducible human lung adenocarcinoma subtypes in multiple independent patient cohorts. J Clin Oncol. 2006; 24:5079–5090. [PubMed: 17075127]
4. Singh A, Greninger P, Rhodes D, Koopman L, Violette S, Bardeesy N, Settleman J. A gene expression signature associated with “K-Ras addiction” reveals regulators of EMT and tumor cell survival. Cancer Cell. 2009; 15:489–500. [PubMed: 19477428]
5. Skoulidis F, Byers LA, Diao L, Papadimitrakopoulou VA, Tong P, Izzo J, Behrens C, Kadara H, Parra ER, Canales JR, Zhang J, Giri U, Gudikote J, Cortez MA, Yang C, Fan Y, Peyton M, Girard L, Coombes KR, Toniatti C, Heffernan TP, Choi M, Frampton GM, Miller V, Weinstein JN, Herbst RS, Wong KK, Zhang J, Sharma P, Mills GB, Hong WK, Minna JD, Allison JP, Futreal A, Wang J, Wistuba, Heymach JV. Co-occurring genomic alterations define major subsets of KRAS-mutant lung adenocarcinoma with distinct biology, immune profiles, and therapeutic vulnerabilities. Cancer Discov. 2015; 5:860–877. [PubMed: 26069186]
6. Kim HS, Mendiratta S, Kim J, Pecot CV, Larsen JE, Zubovych I, Seo BY, Kim J, Eskiocak B, Chung H, McMillan E, Wu S, De Brabander J, Komurov K, Toombs JE, Wei S, Peyton M, Williams N, Gazdar AF, Posner BA, Brekken RA, Sood AK, Deberardinis RJ, Roth MG, Minna JD, White MA. Systematic identification of molecular subtype-selective vulnerabilities in non-small-cell lung cancer. Cell. 2013; 155:552–566. [PubMed: 24243015]

7. Zheng X, Carstens JL, Kim J, et al. Epithelial-to-mesenchymal transition is dispensable for metastasis but induces chemoresistance in pancreatic cancer. Nature. 2015; 527:525–530. [PubMed: 26560028]

8. Rhodes DR, Kalyana-Sundaram S, Mahavisno V, Varambally R, Yu J, Briggs BB, Barrette TR, Anstet MJ, Kincead-Beal C, Kulkarni P, Varambally S, Ghosh D, Chinnaiyan AM. Oncomine 3.0: genes, pathways, and networks in a collection of 18,000 cancer gene expression profiles. Neoplasia. 2007; 9:166–180. [PubMed: 17356713]

9. Kumar MS, Lu J, Mercer KL, Golub TR, Jacks T. Impaired microRNA processing enhances cellular transformation and tumorigenesis. Nat Genet. 2007; 39:673–677. [PubMed: 17401365]

10. Hatley ME, Patrick DM, Garcia MR, Richardson JA, Bassel-Duby R, van Rooij E, Olson EN. Modulation of K-Ras-dependent lung tumorigenesis by MicroRNA-21. Cancer Cell. 2010; 18:282–293. [PubMed: 20832755]

11. Lu J, Getz G, Miska EA, Alvarez-Saavedra E, Lamb J, Peck D, Sweet-Cordero A, Ebert BL, Mak RH, Ferrando AA, Downing JR, Jacks T, Horvitz HR, Golub TR. MicroRNA expression profiles classify human cancers. Nature. 2005; 435:834–838. [PubMed: 15944708]

12. Johnson SM, Grosshans H, Shingara J, Byrom M, Jarvis R, Cheng A, Labourier E, Reinert KL, Brown D, Slack FJ. RAS is regulated by the let-7 microRNA family. Cell. 2005; 120:635–647. [PubMed: 15766527]

13. Chin LJ, Ratner E, Leng S, Zhai R, Nallur S, Babar I, Muller RU, Straka E, Su L, Burki EA, Crowell RE, Patel R, Kulkarni T, Homer R, Zelterman D, Kidd KK, Zhu Y, Christiani DC, Belinsky SA, Slack FJ, Weidhaas JB. A SNP in a let-7 microRNA complementary site in the KRAS 3′ untranslated region increases non-small cell lung cancer risk. Cancer Res. 2008; 68:8535–8540. [PubMed: 18922928]

14. He L, He X, Lim LP, de Stanchina E, Xuan Z, Liang Y, Xue W, Zender L, Magnus J, Ridzon D, Jackson AL, Linsley PS, Chen C, Lowe SW, Cleary MA, Hannon GJ. A microRNA component of the p53 tumour suppressor network. Nature. 2007; 447:1130–1134. [PubMed: 17554337]

15. Gregory PA, Bert AG, Paterson EL, Barry SC, Tsykin A, Farshid G, Vadas MA, Khew-Goodall Y, Goodall GJ. The miR-200 family and miR-205 regulate epithelial to mesenchymal transition by targeting ZEB1 and SIP1. Nat Cell Biol. 2008; 10:593–601. [PubMed: 18376396]

16. Schmittgen TD. Real-time quantitative PCR. Methods. 2001; 25:383–385. [PubMed: 11846607]

17. Chaffer CL, Marjanovic ND, Lee T, Bell G, Kleer CG, Reinhardt F, D'Alessio AC, Young RA, Weinberg RA. Poised chromatin at the ZEB1 promoter enables breast cancer cell plasticity and enhances tumorigenicity. Cell. 2013; 154:61–74. [PubMed: 23827675]

18. Kabbout M, Garcia MM, Fujimoto J, Liu DD, Woods D, Chow CW, Mendoza G, Momin AA, James BP, Solis L, Behrens C, Lee JJ, Wistuba, Kadara H. ETS2 mediated tumor suppressive function and MET oncogene inhibition in human non-small cell lung cancer. Clin Cancer Res. 2013; 19:3383–3395. [PubMed: 23659968]

19. O'Brien J, Wilson I, Orton T, Pognan F. Investigation of the Alamar Blue (resazurin) fluorescent dye for the assessment of mammalian cell cytotoxicity. Eur J Biochem. 2000; 267:5421–5426. [PubMed: 10951200]

20. Guo JY, Chen HY, Mathew R, Fan J, Strohecker AM, Karsli-Uzunbas G, Kamphorst JJ, Chen G, Lemons JM, Karantza V, Coller HA, Dipaola RS, Gelinas C, Rabinowitz JD, White E. Activated Ras requires autophagy to maintain oxidative metabolism and tumorigenesis. Genes Dev. 2011; 25:460–470. [PubMed: 21317241]

21. Klionsky DJ, Abdalla FC, Abeliovich H, Abraham RT, Acevedo-Arozena A, Adeli K, Agholme L, Agnello M, Agostinis P, Aguirre-Ghiso JA, Ahn HJ, Ait-Mohamed O, Ait-Si-Ali S, Akematsu T, Akira S, Al-Younes HM, Al-Zeer MA, Albert ML, Albin RL, Alegre-Abarrategui J, Aleo MF, Alirezaei M, Almasan A, Almonte-Becerril M, Amano A, Amaravadi R, Amarnath S, Amer AO, Andrieu-Abadie N, Anantharam V, Ann DK, Anoopkumar-Dukie S, Aoki H, Apostolova N, Arancia G, Aris JP, Asanuma K, Asare NY, Ashida H, Askanas V, Askew DS, Auberger P, Baba M, Backues SK, Baehrecke EH, Bahr BA, Bai XY, Bailly Y, Baiocchi R, Baldini G, Balduini W, Ballabio A, Bamber BA, Bampton ET, Banhegyi G, Bartholomew CR, Bassham DC, Bast RC Jr, Batoko H, Bay BH, Beau I, Bechet DM, Begley TJ, Behl C, Behrends C, Bekri S, Bellaire B, Bendall LJ, Benetti L, Berliocchi L, Bernardi H, Bernassola F, Besteiro S, Bhatia-Kissova I, Bi X, Biard-Piechaczyk M, Blum JS, Boise LH, Bonaldo P, Boone DL, Bornhauser BC, Bortoluci KR,

Bossis I, Bost F, Bourquin JP, Boya P, Boyer-Guittaut M, Bozhkov PV, Brady NR, Brancolini C, Brech A, Brenman JE, Brennand A, Bresnick EH, Brest P, Bridges D, Bristol ML, Brookes PS, Brown EJ, Brumell JH, Brunetti-Pierri N, Brunk UT, Bulman DE, Bultman SJ, Bultynck G, Burbulla LF, Bursch W, Butchar JP, Buzgariu W, Bydlowski SP, Cadwell K, Cahova M, Cai D, Cai J, Cai Q, Calabretta B, Calvo-Garrido J, Camougrand N, Campanella M, Campos-Salinas J, Candi E, Cao L, Caplan AB, Carding SR, Cardoso SM, Carew JS, Carlin CR, Carmignac V, Carneiro LA, Carra S, Caruso RA, Casari G, Casas C, Castino R, Cebollero E, Cecconi F, Celli J, Chaachouay H, Chae HJ, Chai CY, Chan DC, Chan EY, Chang RC, Che CM, Chen CC, Chen GC, Chen GQ, Chen M, Chen Q, Chen SS, Chen W, Chen X, Chen X, Chen X, Chen YG, Chen Y, Chen Y, Chen YJ, Chen Z, Cheng A, Cheng CH, Cheng Y, Cheong H, Cheong JH, Cherry S, Chess-Williams R, Cheung ZH, Chevet E, Chiang HL, Chiarelli R, Chiba T, Chin LS, Chiou SH, Chisari FV, Cho CH, Cho DH, Choi AM, Choi D, Choi KS, Choi ME, Chouaib S, Choubey D, Choubey V, Chu CT, Chuang TH, Chueh SH, Chun T, Chwae YJ, Chye ML, Ciarcia R, Ciriolo MR, Clague MJ, Clark RS, Clarke PG, Clarke R, Codogno P, Coller HA, Colombo MI, Comincini S, Condello M, Condorelli F, Cookson MR, Coombs GH, Coppens I, Corbalan R, Cossart P, Costelli P, Costes S, Coto-Montes A, Couve E, Coxon FP, Cregg JM, Crespo JL, Cronje MJ, Cuervo AM, Cullen JJ, Czaja MJ, D'Amelio M, Darfeuille-Michaud A, Davids LM, Davies FE, De Felici M, de Groot JF, de Haan CA, De Martino L, De Milito A, De Tata V, Debnath J, Degterev A, Dehay B, Delbridge LM, Demarchi F, Deng YZ, Dengjel J, Dent P, Denton D, Deretic V, Desai SD, Devenish RJ, Di Gioacchino M, Di Paolo G, Di Pietro C, Diaz-Araya G, Diaz-Laviada I, Diaz-Meco MT, Diaz-Nido J, Dikic I, Dinesh-Kumar SP, Ding WX, Distelhorst CW, Diwan A, Djavaheri-Mergny M, Dokudovskaya S, Dong Z, Dorsey FC, Dosenko V, Dowling JJ, Doxsey S, Dreux M, Drew ME, Duan Q, Duchosal MA, Duff K, Dugail I, Durbeej M, Duszenko M, Edelstein CL, Edinger AL, Egea G, Eichinger L, Eissa NT, Ekmekcioglu S, El-Deiry WS, Elazar Z, Elgendy M, Ellerby LM, Eng KE, Engelbrecht AM, Engelender S, Erenpreisa J, Escalante R, Esclatine A, Eskelinen EL, Espert L, Espina V, Fan H, Fan J, Fan QW, Fan Z, Fang S, Fang Y, Fanto M, Fanzani A, Farkas T, Farre JC, Faure M, Fechheimer M, Feng CG, Feng J, Feng Q, Feng Y, Fesus L, Feuer R, Figueiredo-Pereira ME, Fimia GM, Fingar DC, Finkbeiner S, Finkel T, Finley KD, Fiorito F, Fisher EA, Fisher PB, Flajolet M, Florez-McClure ML, Florio S, Fon EA, Fornai F, Fortunato F, Fotedar R, Fowler DH, Fox HS, Franco R, Frankel LB, Fransen M, Fuentes JM, Fueyo J, Fujii J, Fujisaki K, Fujita E, Fukuda M, Furukawa RH, Gaestel M, Gailly P, Gajewska M, Galliot B, Galy V, Ganesh S, Ganetzky B, Ganley IG, Gao FB, Gao GF, Gao J, Garcia L, Garcia-Manero G, Garcia-Marcos M, Garmyn M, Gartel AL, Gatti E, Gautel M, Gawriluk TR, Gegg ME, Geng J, Germain M, Gestwicki JE, Gewirtz DA, Ghavami S, Ghosh P, Giammarioli AM, Giatromanolaki AN, Gibson SB, Gilkerson RW, Ginger ML, Ginsberg HN, Golab J, Goligorsky MS, Golstein P, Gomez-Manzano C, Goncu E, Gongora C, Gonzalez CD, Gonzalez R, Gonzalez-Estevez C, Gonzalez-Polo RA, Gonzalez-Rey E, Gorbunov NV, Gorski S, Goruppi S, Gottlieb RA, Gozuacik D, Granato GE, Grant GD, Green KN, Gregorc A, Gros F, Grose C, Grunt TW, Gual P, Guan JL, Guan KL, Guichard SM, Gukovskaya AS, Gukovsky I, Gunst J, Gustafsson AB, Halayko AJ, Hale AN, Halonen SK, Hamasaki M, Han F, Han T, Hancock MK, Hansen M, Harada H, Harada M, Hardt SE, Harper JW, Harris AL, Harris J, Harris SD, Hashimoto M, Haspel JA, Hayashi S, Hazelhurst LA, He C, He YW, Hebert MJ, Heidenreich KA, Helfrich MH, Helgason GV, Henske EP, Herman B, Herman PK, Hetz C, Hilfiker S, Hill JA, Hocking LJ, Hofman P, Hofmann TG, Hohfeld J, Holyoake TL, Hong MH, Hood DA, Hotamisligil GS, Houwerzijl EJ, Hoyer-Hansen M, Hu B, Hu CA, Hu HM, Hua Y, Huang C, Huang J, Huang S, Huang WP, Huber TB, Huh WK, Hung TH, Hupp TR, Hur GM, Hurley JB, Hussain SN, Hussey PJ, Hwang JJ, Hwang S, Ichihara A, Ilkhanizadeh S, Inoki K, Into T, Iovane V, Iovanna JL, Ip NY, Isaka Y, Ishida H, Isidoro C, Isobe K, Iwasaki A, Izquierdo M, Izumi Y, Jaakkola PM, Jaattela M, Jackson GR, Jackson WT, Janji B, Jendrach M, Jeon JH, Jeung EB, Jiang H, Jiang H, Jiang JX, Jiang M, Jiang Q, Jiang X, Jiang X, Jimenez A, Jin M, Jin S, Joe CO, Johansen T, Johnson DE, Johnson GV, Jones NL, Joseph B, Joseph SK, Joubert AM, Juhasz G, Juillerat-Jeanneret L, Jung CH, Jung YK, Kaarniranta K, Kaasik A, Kabuta T, Kadowaki M, Kagedal K, Kamada Y, Kaminskyy VO, Kampinga HH, Kanamori H, Kang C, Kang KB, Kang KI, Kang R, Kang YA, Kanki T, Kanneganti TD, Kanno H, Kanthasamy AG, Kanthasamy A, Karantza V, Kaushal GP, Kaushik S, Kawazoe Y, Ke PY, Kehrl JH, Kelekar A, Kerkhoff C, Kessel DH, Khalil H, Kiel JA, Kiger AA, Kihara A, Kim DR, Kim DH, Kim DH, Kim EK, Kim HR, Kim JS, Kim JH, Kim JC, Kim JK, Kim PK, Kim SW, Kim YS, Kim Y, Kimchi A, Kimmelman AC, King

JS, Kinsella TJ, Kirkin V, Kirshenbaum LA, Kitamoto K, Kitazato K, Klein L, Klimecki WT, Klucken J, Knecht E, Ko BC, Koch JC, Koga H, Koh JY, Koh YH, Koike M, Komatsu M, Kominami E, Kong HJ, Kong WJ, Korolchuk VI, Kotake Y, Koukourakis MI, Kouri Flores JB, Kovacs AL, Kraft C, Krainc D, Kramer H, Kretz-Remy C, Krichevsky AM, Kroemer G, Kruger R, Krut O, Ktistakis NT, Kuan CY, Kucharczyk R, Kumar A, Kumar R, Kumar S, Kundu M, Kung HJ, Kurz T, Kwon HJ, La Spada AR, Lafont F, Lamark T, Landry J, Lane JD, Lapaquette P, Laporte JF, Laszlo L, Lavandero S, Lavoie JN, Layfield R, Lazo PA, Le W, Le Cam L, Ledbetter DJ, Lee AJ, Lee BW, Lee GM, Lee J, Lee JH, Lee M, Lee MS, Lee SH, Leeuwenburgh C, Legembre P, Legouis R, Lehmann M, Lei HY, Lei QY, Leib DA, Leiro J, Lemasters JJ, Lemoine A, Lesniak MS, Lev D, Levenson VV, Levine B, Levy E, Li F, Li JL, Li L, Li S, Li W, Li XJ, Li YB, Li YP, Liang C, Liang Q, Liao YF, Liberski PP, Lieberman A, Lim HJ, Lim KL, Lim K, Lin CF, Lin FC, Lin J, Lin JD, Lin K, Lin WW, Lin WC, Lin YL, Linden R, Lingor P, Lippincott-Schwartz J, Lisanti MP, Liton PB, Liu B, Liu CF, Liu K, Liu L, Liu QA, Liu W, Liu YC, Liu Y, Lockshin RA, Lok CN, Lonial S, Loos B, Lopez-Berestein G, Lopez-Otin C, Lossi L, Lotze MT, Low P, Lu B, Lu B, Lu B, Lu Z, Luciano F, Lukacs NW, Lund AH, Lynch-Day MA, Ma Y, Macian F, MacKeigan JP, Macleod KF, Madeo F, Maiuri L, Maiuri MC, Malagoli D, Malicdan MC, Malorni W, Man N, Mandelkow EM, Manon S, Manov I, Mao K, Mao X, Mao Z, Marambaud P, Marazziti D, Marcel YL, Marchbank K, Marchetti P, Marciniak SJ, Marcondes M, Mardi M, Marfe G, Marino G, Markaki M, Marten MR, Martin SJ, Martinand-Mari C, Martinet W, Martinez-Vicente M, Masini M, Matarrese P, Matsuo S, Matteoni R, Mayer A, Mazure NM, McConkey DJ, McConnell MJ, McDermott C, McDonald C, McInerney GM, McKenna SL, McLaughlin B, McLean PJ, McMaster CR, McQuibban GA, Meijer AJ, Meisler MH, Melendez A, Melia TJ, Melino G, Mena MA, Menendez JA, Menna-Barreto RF, Menon MB, Menzies FM, Mercer CA, Merighi A, Merry DE, Meschini S, Meyer CG, Meyer TF, Miao CY, Miao JY, Michels PA, Michiels C, Mijaljica D, Milojkovic A, Minucci S, Miracco C, Miranti CK, Mitroulis I, Miyazawa K, Mizushima N, Mograbi B, Mohseni S, Molero X, Mollereau B, Mollinedo F, Momoi T, Monastyrska I, Monick MM, Monteiro MJ, Moore MN, Mora R, Moreau K, Moreira PI, Moriyasu Y, Moscat J, Mostowy S, Mottram JC, Motyl T, Moussa CE, Muller S, Muller S, Munger K, Munz C, Murphy LO, Murphy ME, Musaro A, Mysorekar I, Nagata E, Nagata K, Nahimana A, Nair U, Nakagawa T, Nakahira K, Nakano H, Nakatogawa H, Nanjundan M, Naqvi NI, Narendra DP, Narita M, Navarro M, Nawrocki ST, Nazarko TY, Nemchenko A, Netea MG, Neufeld TP, Ney PA, Nezis IP, Nguyen HP, Nie D, Nishino I, Nislow C, Nixon RA, Noda T, Noegel AA, Nogalska A, Noguchi S, Notterpek L, Novak I, Nozaki T, Nukina N, Nurnberger T, Nyfeler B, Obara K, Oberley TD, Oddo S, Ogawa M, Ohashi T, Okamoto K, Oleinick NL, Oliver FJ, Olsen LJ, Olsson S, Opota O, Osborne TF, Ostrander GK, Otsu K, Ou JH, Ouimet M, Overholtzer M, Ozpolat B, Paganetti P, Pagnini U, Pallet N, Palmer GE, Palumbo C, Pan T, Panaretakis T, Pandey UB, Papackova Z, Papassideri I, Paris I, Park J, Park OK, Parys JB, Parzych KR, Patschan S, Patterson C, Pattingre S, Pawelek JM, Peng J, Perlmutter DH, Perrotta I, Perry G, Pervaiz S, Peter M, Peters GJ, Petersen M, Petrovski G, Phang JM, Piacentini M, Pierre P, Pierrefite-Carle V, Pierron G, Pinkas-Kramarski R, Piras A, Piri N, Platanias LC, Poggeler S, Poirot M, Poletti A, Pous C, Pozuelo-Rubio M, Praetorius-Ibba M, Prasad A, Prescott M, Priault M, Produit-Zengaffinen N, Progulske-Fox A, Proikas-Cezanne T, Przedborski S, Przyklenk K, Puertollano R, Puyal J, Qian SB, Qin L, Qin ZH, Quaggin SE, Raben N, Rabinowich H, Rabkin SW, Rahman I, Rami A, Ramm G, Randall G, Randow F, Rao VA, Rathmell JC, Ravikumar B, Ray SK, Reed BH, Reed JC, Reggiori F, Regnier-Vigouroux A, Reichert AS, Reiners JJ Jr, Reiter RJ, Ren J, Revuelta JL, Rhodes CJ, Ritis K, Rizzo E, Robbins J, Roberge M, Roca H, Roccheri MC, Rocchi S, Rodemann HP, Rodriguez de Cordoba S, Rohrer B, Roninson IB, Rosen K, Rost-Roszkowska MM, Rouis M, Rouschop KM, Rovetta F, Rubin BP, Rubinsztein DC, Ruckdeschel K, Rucker EB 3rd, Rudich A, Rudolf E, Ruiz-Opazo N, Russo R, Rusten TE, Ryan KM, Ryter SW, Sabatini DM, Sadoshima J, Saha T, Saitoh T, Sakagami H, Sakai Y, Salekdeh GH, Salomoni P, Salvaterra PM, Salvesen G, Salvioli R, Sanchez AM, Sanchez-Alcazar JA, Sanchez-Prieto R, Sandri M, Sankar U, Sansanwal P, Santambrogio L, Saran S, Sarkar S, Sarwal M, Sasakawa C, Sasnauskiene A, Sass M, Sato K, Sato M, Schapira AH, Scharl M, Schatzl HM, Scheper W, Schiaffino S, Schneider C, Schneider ME, Schneider-Stock R, Schoenlein PV, Schorderet DF, Schuller C, Schwartz GK, Scorrano L, Sealy L, Seglen PO, Segura-Aguilar J, Seiliez I, Seleverstov O, Sell C, Seo JB, Separovic D, Setaluri V, Setoguchi T, Settembre C, Shacka JJ, Shanmugam M, Shapiro IM, Shaulian E, Shaw RJ, Shelhamer JH, Shen HM, Shen WC, Sheng ZH, Shi Y, Shibuya

K, Shidoji Y, Shieh JJ, Shih CM, Shimada Y, Shimizu S, Shintani T, Shirihai OS, Shore GC, Sibirny AA, Sidhu SB, Sikorska B, Silva-Zacarin EC, Simmons A, Simon AK, Simon HU, Simone C, Simonsen A, Sinclair DA, Singh R, Sinha D, Sinicrope FA, Sirko A, Siu PM, Sivridis E, Skop V, Skulachev VP, Slack RS, Smaili SS, Smith DR, Soengas MS, Soldati T, Song X, Sood AK, Soong TW, Sotgia F, Spector SA, Spies CD, Springer W, Srinivasula SM, Stefanis L, Steffan JS, Stendel R, Stenmark H, Stephanou A, Stern ST, Sternberg C, Stork B, Stralfors P, Subauste CS, Sui X, Sulzer D, Sun J, Sun SY, Sun ZJ, Sung JJ, Suzuki K, Suzuki T, Swanson MS, Swanton C, Sweeney ST, Sy LK, Szabadkai G, Tabas I, Taegtmeyer H, Tafani M, Takacs-Vellai K, Takano Y, Takegawa K, Takemura G, Takeshita F, Talbot NJ, Tan KS, Tanaka K, Tanaka K, Tang D, Tang D, Tanida I, Tannous BA, Tavernarakis N, Taylor GS, Taylor GA, Taylor JP, Terada LS, Terman A, Tettamanti G, Thevissen K, Thompson CB, Thorburn A, Thumm M, Tian F, Tian Y, Tocchini-Valentini G, Tolkovsky AM, Tomino Y, Tonges L, Tooze SA, Tournier C, Tower J, Towns R, Trajkovic V, Travassos LH, Tsai TF, Tschan MP, Tsubata T, Tsung A, Turk B, Turner LS, Tyagi SC, Uchiyama Y, Ueno T, Umekawa M, Umemiya-Shirafuji R, Unni VK, Vaccaro MI, Valente EM, Van den Berghe G, van der Klei IJ, van Doorn W, van Dyk LF, van Egmond M, van Grunsven LA, Vandenabeele P, Vandenberghe WP, Vanhorebeek I, Vaquero EC, Velasco G, Vellai T, Vicencio JM, Vierstra RD, Vila M, Vindis C, Viola G, Viscomi MT, Voitsekhovskaja OV, von Haefen C, Votruba M, Wada K, Wade-Martins R, Walker CL, Walsh CM, Walter J, Wan XB, Wang A, Wang C, Wang D, Wang F, Wang F, Wang G, Wang H, Wang HG, Wang HD, Wang J, Wang K, Wang M, Wang RC, Wang X, Wang X, Wang YJ, Wang Y, Wang Z, Wang ZC, Wang Z, Wansink DG, Ward DM, Watada H, Waters SL, Webster P, Wei L, Weihl CC, Weiss WA, Welford SM, Wen LP, Whitehouse CA, Whitton JL, Whitworth AJ, Wileman T, Wiley JW, Wilkinson S, Willbold D, Williams RL, Williamson PR, Wouters BG, Wu C, Wu DC, Wu WK, Wyttenbach A, Xavier RJ, Xi Z, Xia P, Xiao G, Xie Z, Xie Z, Xu DZ, Xu J, Xu L, Xu X, Yamamoto A, Yamamoto A, Yamashina S, Yamashita M, Yan X, Yanagida M, Yang DS, Yang E, Yang JM, Yang SY, Yang W, Yang WY, Yang Z, Yao MC, Yao TP, Yeganeh B, Yen WL, Yin JJ, Yin XM, Yoo OJ, Yoon G, Yoon SY, Yorimitsu T, Yoshikawa Y, Yoshimori T, Yoshimoto K, You HJ, Youle RJ, Younes A, Yu L, Yu L, Yu SW, Yu WH, Yuan ZM, Yue Z, Yun CH, Yuzaki M, Zabirnyk O, Silva-Zacarin E, Zacks D, Zacksenhaus E, Zaffaroni N, Zakeri Z, Zeh HJ 3rd, Zeitlin SO, Zhang H, Zhang HL, Zhang J, Zhang JP, Zhang L, Zhang L, Zhang MY, Zhang XD, Zhao M, Zhao YF, Zhao Y, Zhao ZJ, Zheng X, Zhivotovsky B, Zhong Q, Zhou CZ, Zhu C, Zhu WG, Zhu XF, Zhu X, Zhu Y, Zoladek T, Zong WX, Zorzano A, Zschocke J, Zuckerbraun B. Guidelines for the use and interpretation of assays for monitoring autophagy. Autophagy. 2012; 8:445–544. [PubMed: 22966490]

22. N'Diaye EN, Kajihara KK, Hsieh I, Morisaki H, Debnath J, Brown EJ. PLIC proteins or ubiquilins regulate autophagy-dependent cell survival during nutrient starvation. EMBO Rep. 2009; 10:173–179. [PubMed: 19148225]
23. Sanjuan MA, Dillon CP, Tait SW, Moshiach S, Dorsey F, Connell S, Komatsu M, Tanaka K, Cleveland JL, Withoff S, Green DR. Toll-like receptor signalling in macrophages links the autophagy pathway to phagocytosis. Nature. 2007; 450:1253–1257. [PubMed: 18097414]
24. Pankiv S, Clausen TH, Lamark T, Brech A, Bruun JA, Outzen H, Overvatn A, Bjorkoy G, Johansen T. p62/SQSTM1 binds directly to Atg8/LC3 to facilitate degradation of ubiquitinated protein aggregates by autophagy. The Journal of biological chemistry. 2007; 282:24131–24145. [PubMed: 17580304]
25. Kang R, Zeh HJ, Lotze MT, Tang D. The Beclin 1 network regulates autophagy and apoptosis. Cell death and differentiation. 2011; 18:571–580. [PubMed: 21311563]
26. Matsunaga K, Saitoh T, Tabata K, Omori H, Satoh T, Kurotori N, Maejima I, Shirahama-Noda K, Ichimura T, Isobe T, Akira S, Noda T, Yoshimori T. Two Beclin 1-binding proteins, Atg14L and Rubicon, reciprocally regulate autophagy at different stages. Nat Cell Biol. 2009; 11:385–396. [PubMed: 19270696]
27. Jiang T, Qin B, He J, Lin S, Ding S. Three isoforms of the Atg16L1 protein contribute different autophagic properties. Mol Cell Biochem. 2013; 378:257–266. [PubMed: 23512522]
28. Kirkin V, Lamark T, Sou YS, Bjorkoy G, Nunn JL, Bruun JA, Shvets E, McEwan DG, Clausen TH, Wild P, Bilusic I, Theurillat JP, Overvatn A, Ishii T, Elazar Z, Komatsu M, Dikic I, Johansen T. A role for NBR1 in autophagosomal degradation of ubiquitinated substrates. Mol Cell. 2009; 33:505–516. [PubMed: 19250911]

29. Karin M. The beginning of the end: IkappaB kinase (IKK) and NF-kappaB activation. The Journal of biological chemistry. 1999; 274:27339–27342. [PubMed: 10488062]
30. Kawai T, Akira S. Signaling to NF-kappaB by Toll-like receptors. Trends Mol Med. 2007; 13:460–469. [PubMed: 18029230]
31. Perera RM, Stoykova S, Nicolay BN, Ross KN, Fitamant J, Boukhali M, Lengrand J, Deshpande V, Selig MK, Ferrone CR, Settleman J, Stephanopoulos G, Dyson NJ, Zoncu R, Ramaswamy S, Haas W, Bardeesy N. Transcriptional control of autophagy-lysosome function drives pancreatic cancer metabolism. Nature. 2015; 524:361–365. [PubMed: 26168401]
32. Yang S, Wang X, Contino G, Liesa M, Sahin E, Ying H, Bause A, Li Y, Stommel JM, Dell'antonio G, Mautner J, Tonon G, Haigis M, Shirihai OS, Doglioni C, Bardeesy N, Kimmelman AC. Pancreatic cancers require autophagy for tumor growth. Genes Dev. 2011; 25:717–729. [PubMed: 21406549]
33. Moscat J, Diaz-Meco MT. p62 at the crossroads of autophagy, apoptosis, and cancer. Cell. 2009; 137:1001–1004. [PubMed: 19524504]
34. Green DR, Levine B. To be or not to be? How selective autophagy and cell death govern cell fate. Cell. 2014; 157:65–75. [PubMed: 24679527]
35. Duran A, Linares JF, Galvez AS, Wikenheiser K, Flores JM, Diaz-Meco MT, Moscat J. The signaling adaptor p62 is an important NF-kappaB mediator in tumorigenesis. Cancer Cell. 2008; 13:343–354. [PubMed: 18394557]
36. Moscat J, Karin M, Diaz-Meco MT. p62 in Cancer: Signaling Adaptor Beyond Autophagy. Cell. 2016; 167:606–609. [PubMed: 27768885]
37. Qu X, Yu J, Bhagat G, Furuya N, Hibshoosh H, Troxel A, Rosen J, Eskelinen EL, Mizushima N, Ohsumi Y, Cattoretti G, Levine B. Promotion of tumorigenesis by heterozygous disruption of the beclin 1 autophagy gene. J Clin Invest. 2003; 112:1809–1820. [PubMed: 14638851]
38. Jegga AG, Schneider L, Ouyang X, Zhang J. Systems biology of the autophagy-lysosomal pathway. Autophagy. 2011; 7:477–489. [PubMed: 21293178]
39. Wang RC, Wei Y, An Z, Zou Z, Xiao G, Bhagat G, White M, Reichelt J, Levine B. Akt-mediated regulation of autophagy and tumorigenesis through Beclin 1 phosphorylation. Science. 2012; 338:956–959. [PubMed: 23112296]
40. Jaber N, Dou Z, Chen JS, Catanzaro J, Jiang YP, Ballou LM, Selinger E, Ouyang X, Lin RZ, Zhang J, Zong WX. Class III PI3K Vps34 plays an essential role in autophagy and in heart and liver function. Proc Natl Acad Sci U S A. 2012; 109:2003–2008. [PubMed: 22308354]
41. Salas E, Roy S, Marsh T, Rubin B, Debnath J. Oxidative pentose phosphate pathway inhibition is a key determinant of antimalarial induced cancer cell death. Oncogene. 2016; 35:2913–2922. [PubMed: 26434592]
42. Valencia T, Kim JY, Abu-Baker S, Moscat-Pardos J, Ahn CS, Reina-Campos M, Duran A, Castilla EA, Metallo CM, Diaz-Meco MT, Moscat J. Metabolic reprogramming of stromal fibroblasts through p62-mTORC1 signaling promotes inflammation and tumorigenesis. Cancer Cell. 2014; 26:121–135. [PubMed: 25002027]
43. Olarerin-George AO, Anton L, Hwang YC, Elovitz MA, Hogenesch JB. A functional genomics screen for microRNA regulators of NF-kappaB signaling. BMC Biol. 2013; 11:19. [PubMed: 23448136]
44. Hampe J, Franke A, Rosenstiel P, Till A, Teuber M, Huse K, Albrecht M, Mayr G, De La Vega FM, Briggs J, Gunther S, Prescott NJ, Onnie CM, Hasler R, Sipos B, Folsch UR, Lengauer T, Platzer M, Mathew CG, Krawczak M, Schreiber S. A genome-wide association scan of nonsynonymous SNPs identifies a susceptibility variant for Crohn disease in ATG16L1. Nat Genet. 2007; 39:207–211. [PubMed: 17200669]
45. Trang P, Wiggins JF, Daige CL, Cho C, Omotola M, Brown D, Weidhaas JB, Bader AG, Slack FJ. Systemic delivery of tumor suppressor microRNA mimics using a neutral lipid emulsion inhibits lung tumors in mice. Mol Ther. 2011; 19:1116–1122. [PubMed: 21427705]
46. Chan E, Patel R, Nallur S, Ratner E, Bacchiocchi A, Hoyt K, Szpakowski S, Godshalk S, Ariyan S, Sznol M, Halaban R, Krauthammer M, Tuck D, Slack FJ, Weidhaas JB. MicroRNA signatures differentiate melanoma subtypes. Cell Cycle. 2011; 10:1845–1852. [PubMed: 21543894]

47. Garnett MJ, Edelman EJ, Heidorn SJ, Greenman CD, Dastur A, Lau KW, Greninger P, Thompson IR, Luo X, Soares J, Liu Q, Iorio F, Surdez D, Chen L, Milano RJ, Bignell GR, Tam AT, Davies H, Stevenson JA, Barthorpe S, Lutz SR, Kogera F, Lawrence K, McLaren-Douglas A, Mitropoulos X, Mironenko T, Thi H, Richardson L, Zhou W, Jewitt F, Zhang T, O'Brien P, Boisvert JL, Price S, Hur W, Yang W, Deng X, Butler A, Choi HG, Chang JW, Baselga J, Stamenkovic I, Engelman JA, Sharma SV, Delattre O, Saez-Rodriguez J, Gray NS, Settleman J, Futreal PA, Haber DA, Stratton MR, Ramaswamy S, McDermott U, Benes CH. Systematic identification of genomic markers of drug sensitivity in cancer cells. Nature. 2012; 483:570–575. [PubMed: 22460902]

48. Singh A, Sweeney MF, Yu M, Burger A, Greninger P, Benes C, Haber DA, Settleman J. TAK1 inhibition promotes apoptosis in KRAS-dependent colon cancers. Cell. 2012; 148:639–650. [PubMed: 22341439]

49. Lee GY, Kenny PA, Lee EH, Bissell MJ. Three-dimensional culture models of normal and malignant breast epithelial cells. Nature methods. 2007; 4:359–365. [PubMed: 17396127]

50. Carpenter AE, Jones TR, Lamprecht MR, Clarke C, Kang IH, Friman O, Guertin DA, Chang JH, Lindquist RA, Moffat J, Golland P, Sabatini DM. CellProfiler: image analysis software for identifying and quantifying cell phenotypes. Genome Biol. 2006; 7:R100. [PubMed: 17076895]

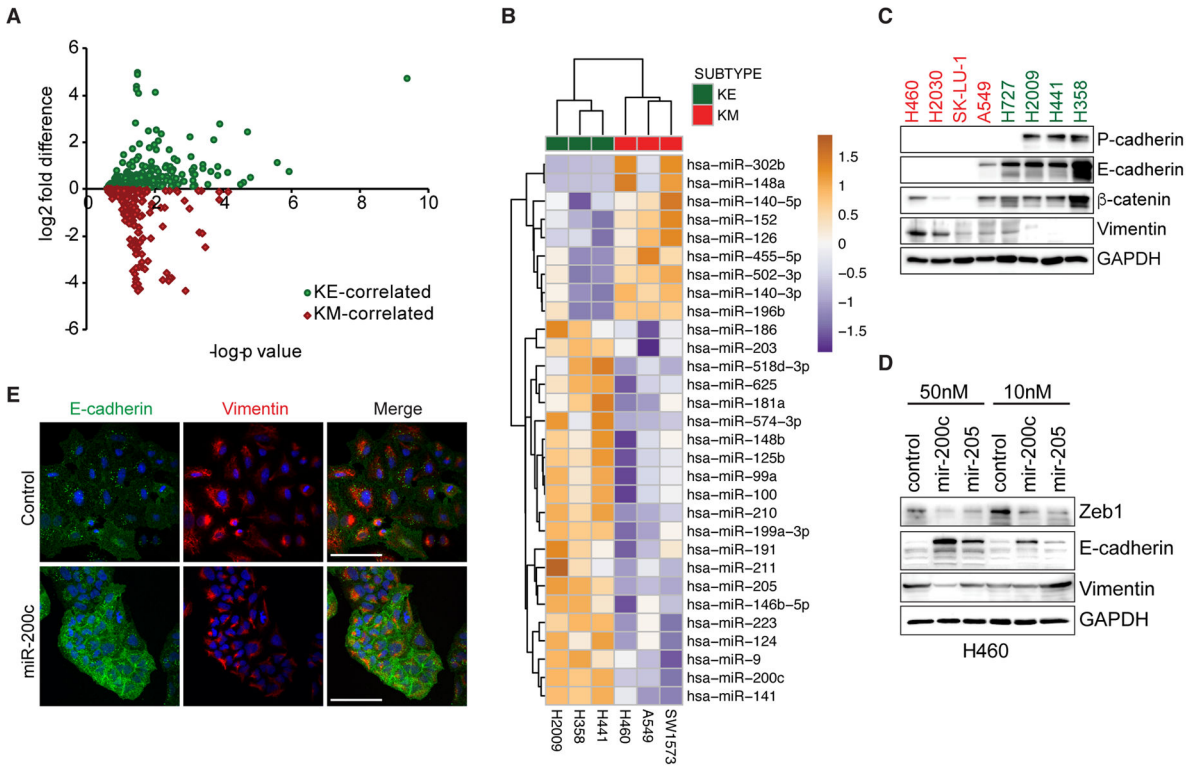

Fig. 1.

KRAS oncogene dependency and epithelial-mesenchymal phenotypes are associated with a miRNA expression signature in NSCLC cell lines. (**A**) Volcano plot of differential miRNA expression based on qPCR-based profiling in six representative *KRAS* mutant NSCLC cell lines. Fold expression differences were calculated by comparing average expression levels in three KRAS dependent/epithelial (KE-correlated) to three KRAS independent/mesenchymal (KM-correlated) cell lines. Student t test derived p values are plotted on a –log scale on the horizontal axis (2-sided test with unequal variances). (**B**) Heat map representation of differential miRNA expression levels ($p < 0.1$) in KE versus KM subtype cell lines, as used in the volcano plot in (A). Orange and purple indicate high and low median-centered expression levels, respectively. Cell lines and miRNAs are clustered by similarity as determined by Euclidean distance. (**C**) Western blotting for abundance of epithelial markers (P-cadherin, E-cadherin and β-catenin) and vimentin as a mesenchymal marker in a panel of KM (red text) and KE (green text) NSCLC cell lines. GAPDH serves as a gel loading control for panels D and E. (**D**) Western blot showing effects of miR-200c and miR-205 reconstitution in H460 KM cells at two concentrations of synthetic mimic oligonucleotides (10 and 50nM) on the abundance of epithelial and mesenchymal markers. Data are representative of 2 independent experiments. (**E)** Confocal immunofluorescence micrographs of H460 cells transfected with control or miR-200c mimics. Cells are shown co-stained with E-cadherin (green channel) and vimentin (red channel). Scale bar, 25μM.

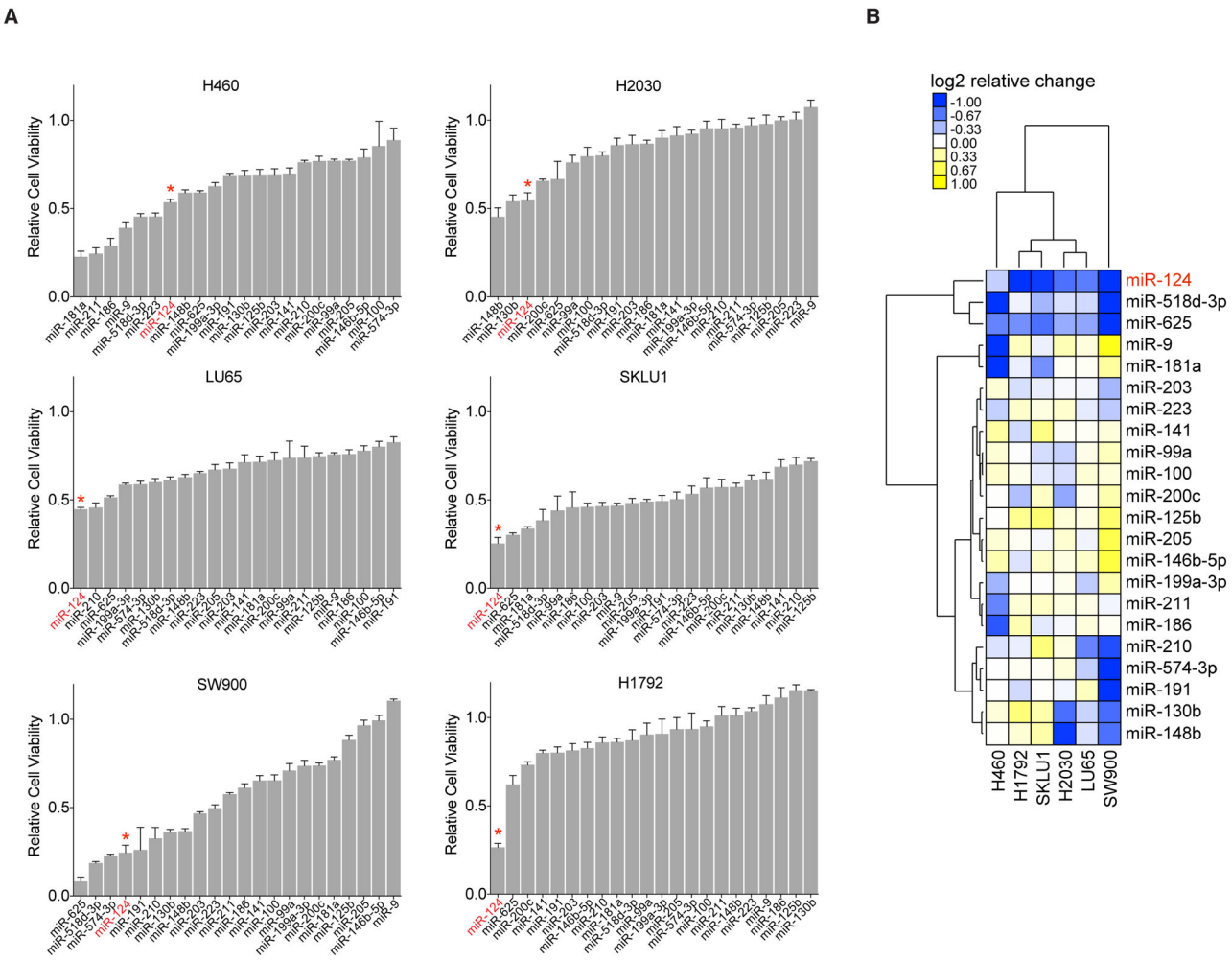

Fig. 2.

Reconstitution of specific KE-correlated miRNAs causes reduced cell viability in KM cell lines. (**A**) Alamar-blue based cell proliferation/viability assays measuring relative viability of indicated cell lines following transfection with 10nM synthetic miRNA mimic oligonucleotides compared to NC control transfected cells 72 h post-transfection. Data are mean of 3 replicates +/- SEM. Viability effects of miR-124 are highlighted with a red asterisk. (**B**) Heat map representing normalized median-centered viability data from (A). Cell lines and miRNAs are clustered by a Euclidean distance similarity metric. MiR-124 is highlighted in red text.

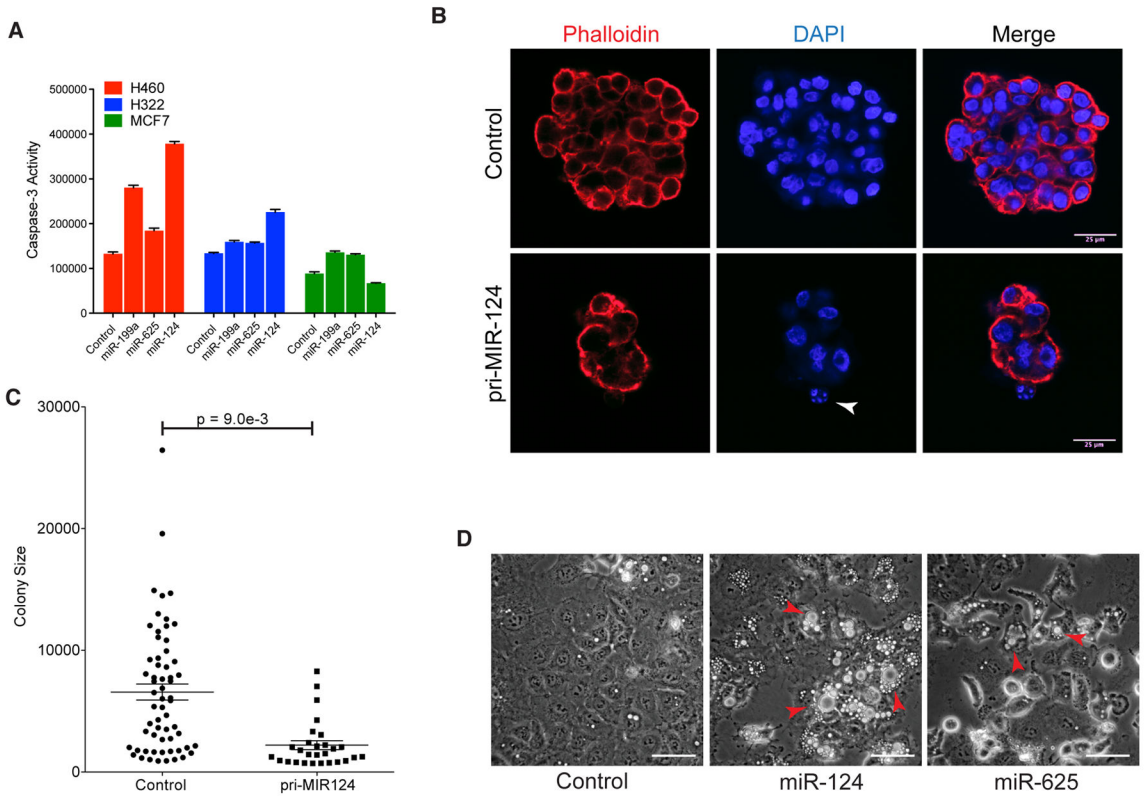

Fig. 3.

MiR-124 reconstitution causes cytotoxic effects in KM cell lines. (**A**) Luciferase-based caspase-3 activation assays following reconstitution of indicated miRNA mimics in H460 KM cells, H322 *KRAS-WT* NSCLC cells and MCF7 *KRAS-WT* breast cancer cells. (**B**) 3D Matrigel™ assays of A549 KM cell growth following lentiviral expression of control luciferase (LUC) or primary MIR124 (pri-MIR124). Fixed cells are shown stained with phalloidin to visualize actin filaments (red signal) and DAPI to visualize nuclear DNA (blue signal). Arrow indicates an apoptotic cell with fragmented DNA and low actin content. Scale bar = 25μm. (**C**) Automated image-based quantitation of colony size and number from 3D Matrigel assays shown in panel B. Colony size is in arbitrary pixel units. Bars represent population means +/- SEM. (**D**) Bright field microscopy images of NC control or miRNA transfected cells. Arrows indicate large intracellular endosomal, possibly vacuolar structures. Scale bar = 25μm. Data are representative of 3 independent experiments.

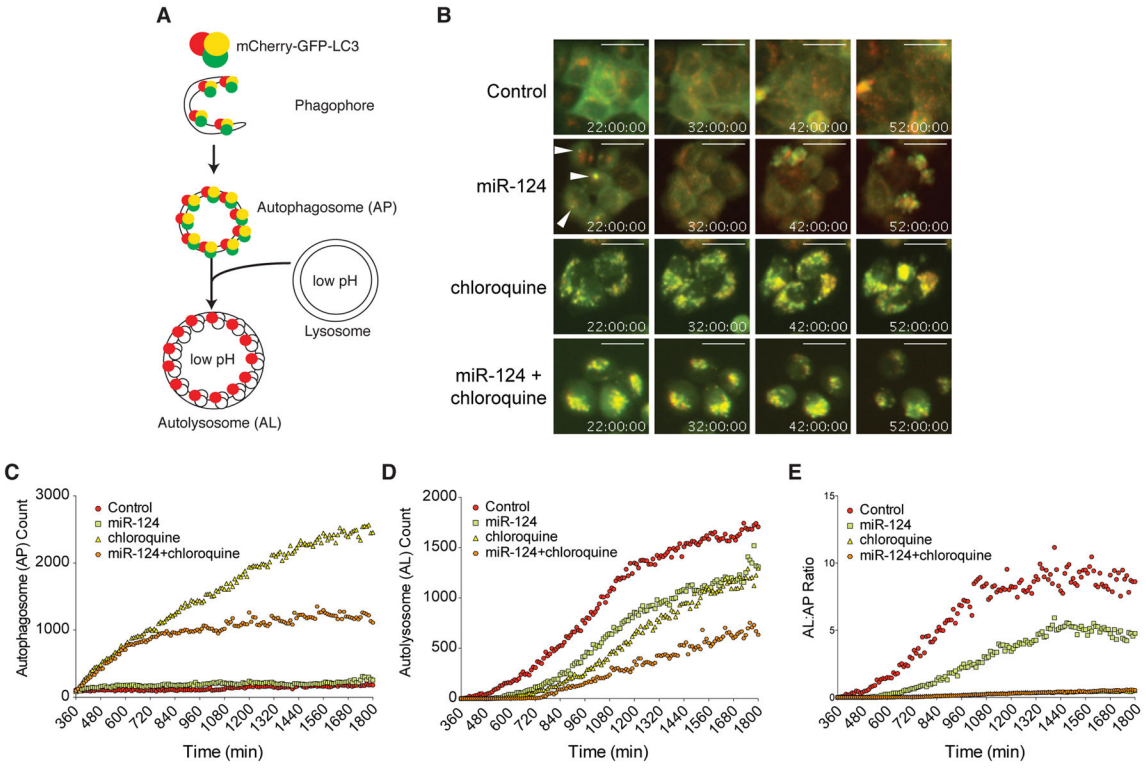

Fig. 4.

MiR-124 reconstitution blocks autolysosome accumulation in KM cells. (**A**) Schematic overview of the mCherry-GFP-LC3 reporter. (**B**) Live cell imaging of H460 KM cells expressing the mCherry-GFP-LC3 reporter and transfected with miR-124 oligonucleotide dsRNA and/or treated with 50μM chloroquine. Arrows indicate LC3 aggregates that are GFP and mCherry double-positive, indicative of phagophore or autophagosome accumulation. Time is shown in hours. Scale bar = 25μm. (**C**) Quantitation of GFP/mCherry double-positive puncta, indicating phagophores/autophagosomes (AP) using image analysis software (BioTek Gen5). (**D**) Quantitation of mCherry positive autolysosomes (AL). (**E**) Quantitation of AL:AP ratio. Data are representative of 3 independent experiments.

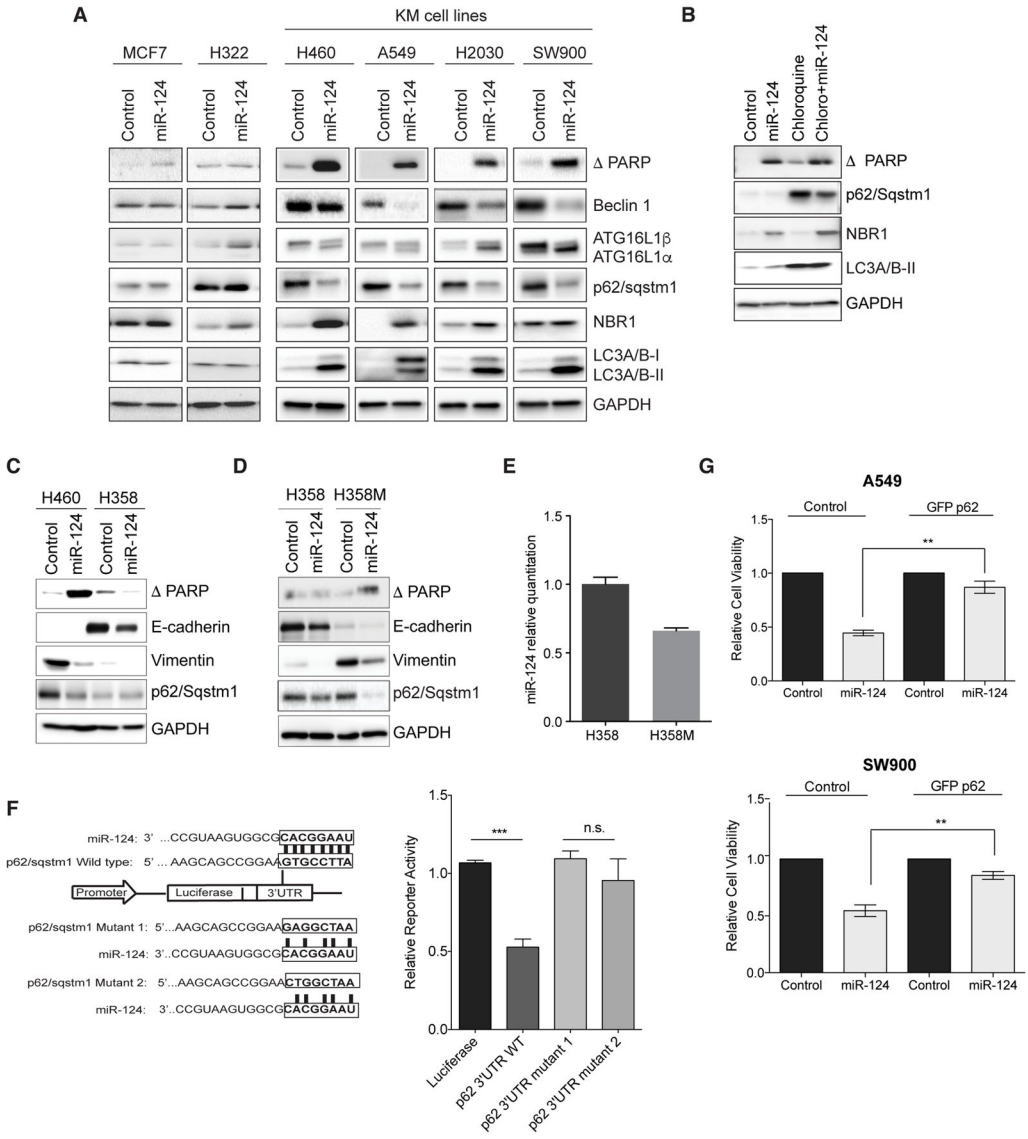

Fig. 5.

MiR-124 reconstitution represses beclin 1 and p62 expression selectively in KM cells. (**A**) Western blot showing protein expression levels of cleaved PARP, indicative of apoptosis, and autophagy pathway components Beclin 1, ATG16L1 α/β splice isoforms, p62 and LC3-I/II following transfection with miR-124 in 2 KRAS WT cell lines (MCF7 and H322) and 4 KM cell lines. GAPDH is a gel loading control. (**B**) Western blot analysis of effects of miR-124 transfection minus/plus chloroquine treatment on expression levels of p62, NBR1 and LC3-II in H460 cells. (**C**) Western blot showing indicated protein levels following miR-124 reconstitution in H460 KM cells compared to H358 KE cells. Cleaved (Δ) PARP indicates apoptosis. E-cadherin and vimentin indicate epithelial versus mesenchymal differentiation. **(D)** Western blot analysis of cleaved PARP, E-cadherin, vimentin and p62 in H358 KE cells compared to a stable mesenchymal derivative cell line H358M, following miR-124 transfection. GAPDH serves as a gel loading control for panels A, B, C and F. (**E**) Quantitation of endogenous mature miR-124 levels by qPCR in H358M cells relative to

parental H358 cells. ** $p < 0.005$ (**F**) Schematic representation of the human *p62/SQSTM1* 3′UTR showing the miR-124 binding site seed sequence and point mutants (1 and 2) that disrupt the miR-124/*SQSTM1* interaction. Reporter activity of wild-type or mutant *SQSTM1* 3′ UTRs following miR-124 transfection. Data are the mean of 3 replicates + SEM. *** $p < 0.0005$; n.s. = not significant. (**G**) Rescue of miR-124 induced cell viability defects with exogenous GFP-tagged p62 expression in A549 and SW900 KM cell lines. Data are the mean of 3 replicates +/- SEM. ** $p < 0.005$. All data are representative of 3 independent experiments.

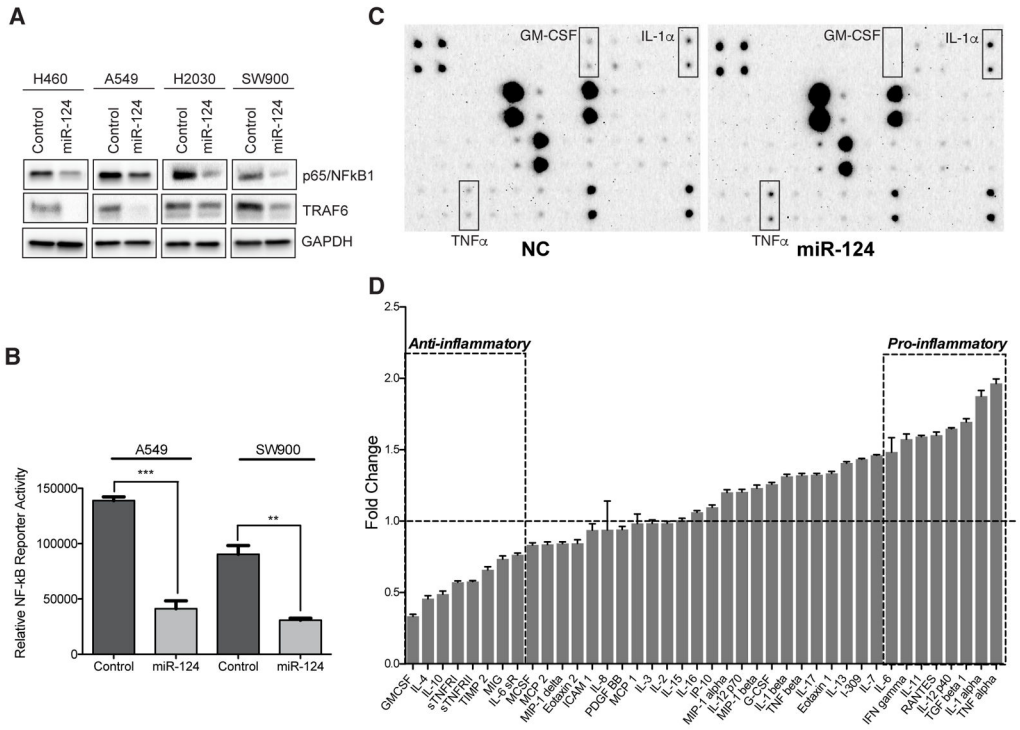

Fig. 6.

MiR-124 reconstitution induces altered expression of NF-κB regulated inflammatory cytokines. (**A**) Western blots showing protein expression levels of the p65 (RELA) subunit of NF-κB and TRAF6 following miR-124 reconstitution in the indicated KM cell lines. GAPDH is a gel loading control. (**B**) NF-κB dependent luciferase reporter assays showing arbitrary luminescence counts following control NC or miR-124 transfection in A549 and SW900 KM cells. *** $p<0.0005$; ** $p<0.005$ (**C**) Antibody-based proteomics array showing expression levels of inflammatory cytokines in conditioned media from NC or miR-124 transfected H460 KM cells. Most significantly altered cytokines are highlighted in boxes. (**D**) Relative quantitation of pixel density from arrays shown in (C), comparing miR-124 to NC control transfected cells. Data are representative of 2 independent experiments.

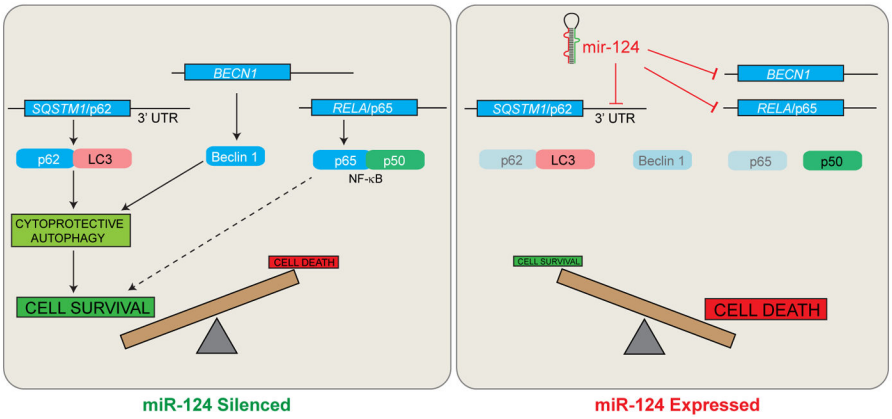

Fig. 7.

A model of miR-124 activity in *KRAS* mutant mesenchymal (KM) cells. In KM cells, under basal conditions, the balance between cell survival and cell death is tightly regulated by autophagy and NF-κB signaling pathways. Upon miR-124 reconstitution in KM cells, abundance of *SQSTM1/p62*, *BECN1*, *TRAF6* and *RELA* are suppressed, causing inhibition of autophagy flux and perturbation of NF-κB signaling. Ultimately, these coordinated miR-124 effects tip the balance in favor of cell death.